1 Title:

2 **Macromolecular Crowding-Affected Mobility of Bcnt/Cfdp1, a Disordered Component of**
3 **the Srcap Complex, from the Nucleus to Cytosol in Subcellular Fractionation**

Authors:

Shintaro Iwashita[1,2, †, *], Takehiro Suzuki[3, †], Kouichi Nishimura[4], Ayaka Onishi[1], Kyoka Tsukuda[2,5,¶], Yoshito Kakihara[6], Yoshimitsu Kiriyama[1,2], Yoshiharu Ohoka[1], Kentaro Nakashima[1,2*]

Authors and Affiliations

[1] Kagawa School of Pharmaceutical Sciences, Tokushima Bunri University, Kagawa, 769-2193, Japan[§]

[2] Institute of Neuroscience, Tokushima Bunri University, Kagawa, 769-2193, Japan[§]

[3] Biomolecular Characterization Unit, RIKEN Center for Sustainable Resource Science, Saitama 351-0198, Japan

[4] Graduate School of Biomedical Science, Tokushima University, Tokushima, 770-8503, Japan

[5] Graduate School of Pharmaceutical Sciences, Tokushima Bunri University, Kagawa, 769-2193, Japan[§]

[6] Division of Dental Pharmacology, Niigata University Graduate School of Medical and Dental Sciences, Niigata, 951-8514, Japan

[¶]Present address: Department of Pharmacy, Faculty of Pharmacy, Kindai University, Osaka, 577-8502, Japan

[†]These authors contributed equally to the analysis.

[§]Tokushima Bunri University at Sanuki City campus moved to Takamatsu City on 1st April 2025. New address: 8-53 Hamanocho, Takamatsu, Kagawa, 760-0011, Japan

* Correspondence: sanukishido1997@gmail.com & nkentaro@kph.bunri-u.ac.jp

Keywords:
Intracellular behavior, Nucleus-cytosol mobility, Western blot, Quantitative proteomic analysis, digitonin, Wnt signaling

4

ABSTRACT

Metazoan *Bucentaur/Craniofacial Development Protein 1* (*Bcnt/Cfdp1*) is crucial for embryonic development, and its yeast homolog protein, SWC5, functions as part of the SWR1 complex in histone exchange reactions. Bcnt/Cfdp1, an intrinsically disordered protein (IDP) subject to various post-translational modifications, contains a putative nuclear localization sequence. Nevertheless, its subcellular localization remains ambiguous. We investigated its intracellular trafficking using diverse approaches. In C2C12 myoblasts, fluorescent protein-tagged Bcnt/Cfdp1 was predominantly localized within the nucleus, preferentially in regions of low DAPI density in myoblasts, and the localization persisted in differentiated multinucleated myotubes. Conversely, detergent-based biochemical fractionation of C2C12 and HEK293T cells indicated a substantial presence of Bcnt/Cfdp1 in cytoplasmic fractions. Quantitative proteomic analysis of fractionated proteins revealed that six IDPs, including a PEST-containing nuclear protein, demonstrated similar distribution patterns to Bcnt/Cfdp1; despite being annotated as nuclear proteins, they were detected in cytoplasmic fractions. Direct treatment of both cell lines with digitonin enabled the collection of released proteins in three steps to accurately isolate cytoplasmic proteins. Bcnt/Cfdp1 exhibited distinct extraction patterns compared to cytoplasmic soluble protein extracts in Ficoll/sucrose solution, while no differences were noted when cells underwent digitonin treatment in an isotonic solution. Quantitative proteomic analysis of these extracts highlighted the mobility or integrity of each protein within the cytoplasm. Consequently, although Bcnt/Cfdp1 is essential within the nucleus, our findings suggest its additional presence in the cytoplasm. We hypothesize that the elastic properties of Bcnt/Cfdp1 facilitate its translocation from the nucleus during subcellular fractionation, which is affected by macromolecular crowding.

INTRODUCTION

Organisms have evolved cellular regulatory systems to maintain sophisticated homeostasis in response to environmental stimuli, such as heat and radiation, and stimuli generated by intracellular biosynthesis, such as oxidative stress. Cellular gene-dependent macromolecules dynamically shuttle between the nucleus and cytoplasm during biosynthesis and are recruited to appropriate cellular compartments with high efficiency in response to intracellular and extracellular stimuli. Recent evidence has revealed that these macromolecular behavior dynamics depend on the generated condensates or liquid-liquid phase separation (LLPS), which allows the inclusion and exclusion of necessary and unnecessary components, respectively [1–3].

Among the myriad cellular macromolecules, intrinsically disordered proteins (IDPs) and proteins containing intrinsically disordered regions (IDRs) have attracted attention in the context of condensate formation. IDPs and IDRs are frequently found as scaffolding proteins with multivalent macromolecules and RNA in condensates, such as stress granules (SGs) and processing bodies (PBs) in the cytoplasm and paraspeckles in the nucleus [4]. It is noteworthy that the subtle structure changes in IDRs, such as modifications through phosphorylation/dephosphorylation, have the potential to regulate condensate formation [3]. The low-density condensates have porous and permeable properties, demonstrated in SGs and nuclear speckles [5], where most molecules move freely while the concentrations of related molecules are high [6].

In the context of nuclear-cytoplasmic transport, the structure of the nuclear membrane, particularly the nuclear pore complex (NPC), the only gate with bidirectional potential between the cytoplasm and nucleus, has been intensively studied; IDP and IDR have also been found to play crucial roles in this process [7]. The two types of nuclear transport mediated by NPCs are classified as active and passive transport, depending on the requirement of receptors and energy. The barrier allows ≤30–60 kDa molecules to pass through passive diffusion, showing its entropy-driven nature rather than geometric constriction [8]. Notably, IDPs can diffuse through the NPC without requiring energy or specific transport receptors, while folded protein transport has been revealed to be size-dependent [9].

From yeast to humans, metazoan Bucentaur/Craniofacial development protein 1 (Bcnt/Cfdp1)[‡] displays a high degree of structural disorder in the N-terminal region and an evolutionarily conserved C-terminal amino acid sequence (BCNT domain) [10]. The yeast ortholog SWC5 is a subunit of the SWR1 (SRCAP in humans) chromatin remodeling complex, SWR1-C (SRCAP-C in humans), while BCNT/CFDP1 has often been treated as an orphan [11, 12]. This is partly due to the failure to capture it as a component of SRCAP-C compared with other subunits [13]. The N-terminal DEY/F motifs of SWC5 engage the canonical histone H2A–H2B [14], whereas the C-terminal BCNT-C domain binds histone H3–H4 and DNA [15] and activates the ATPase of SWR1 [16]. This dual function may contribute to the direction of the torsional force converting the H2A–H2B dimer to H2A.Z–H2B [14–17].

[‡]The official name of *Bcnt/Cfdp1* is *Cfdp**1***. However, genetic studies of disease [1] or transcriptome analysis [2] do not provide solid evidence for its involvement in craniofacial development, including mouse tooth development [3]. Therefore, the nomenclature of *Cfdp1* is misleading and needs to be more accurate. To maintain consistency with previous studies, the term *Bcnt/Cfdp1* rather than *Cfdp1* is used in this article.

SWC5 data, based on genetic information, provide clues for inferring the functional frame of Bcnt/Cfdp1 from a causal perspective (https://www.yeastgenome.org/locus/S000000435) [18]. Although ***SWR1*** and ***SWC5*** are non-essential genes, they play crucial roles under stressful conditions and have versatile functions. SWC5 protein abundance increases in response to DNA replication stress, and each null strain has decreased or increased resistance to certain chemical compounds, which, along with other factors, may affect their lifespan [18]. In addition, tight control of the histone exchange reaction has been demonstrated to be essential for regulating chromatin dynamics [19].

In contrast, *Bcnt/Cfdp1* is essential for metazoan development, as has been demonstrated for the *Drosophila* homolog *Yeti* [20], zebrafish *cfdp1* [21, 22], and mouse *Cfdp1* [23], [https://www.jax.org/strain/033834], suggesting its critical role in pluripotency and differentiation. The following two lines of evidence for *Bcnt/Cfdp1* as a selected gene suggest that it may have versatile functions in homeostasis, similar to *SWC5*. First, it contributes to the persistence of Chinese hamster ovary cell cultures [24] and resistance to Marek's disease in chickens [25]. Perturbation of *Bcnt/Cfdp1* in cells or tissues, whether through gain or loss, has been demonstrated to modulate cell migration, cell cycle progression, and apoptosis/anti-apoptosis [20-22, 26]. These phenotypes are preferentially associated with the Wnt/Notch/Akt signaling pathway [27]. Notably, the Wnt signaling pathway is suppressed explicitly in extraluminal mesenchymal cells of the valves of zebrafish Bcnt/Cfdp1-deficient embryos. This defect leads to cardiac dysfunction [22]. Second, *BCNT/CFDP1* has been identified as a prognostic marker for several types of cancers [28, 29]. In addition, Srcap-C has been demonstrated to be involved in a wide range of biological processes, including differentiation [30], DNA damage repair [31], and disease development [32].

We previously reported that *Bcnt/Cfdp1* knockdown at the genomic level in a mouse embryonic stem (ES) cell line, Cfdp1-K1, had a significant impact on the expression of numerous genes, with more than 4% of all genes upregulated or downregulated by more than two-fold [33]. Consistent with this result, RNAi depletion of BCNT/CFDP1 in HeLa cells has been reported to have widespread effects on cellular functions [26]. Of note, this phenomenon may be comparable to the natural genetic variation found in the fission yeast, *swc5*, likely due to the insufficient functionality of the histone exchange reaction [34]. Given that the aforementioned biological phenotypes induced by *Bcnt/Cfdp1* perturbations are preferentially related to the Wnt/Notch/Akt signaling pathway, it seems reasonable to consider that they are indirectly or partially due to perturbations in the Srcap-C transcriptional regulatory framework. This consideration means that while we have gained insight into the function of Bcnt/Cfdp1, we still need more information about its fundamental properties. Assessing the intracellular

102 trafficking of target proteins is essential for understanding fundamental physiological
103 networks and functions, such as cell cycle control [35], and clarifying the causes of
104 diseases [36].
105 Vertebrate Bcnt/Cfdp1 has typical putative nuclear localization sequences in the N-terminal
106 region, such as ^{50}GKKRKAQSIPARKRR^{64} of the human ortholog. However, its subcellular
107 localization remains ambiguous (https://www.proteinatlas.org/ENSG00000153774-
108 CFDP1/subcellular) mainly due to the lack of appropriate antibodies against Bcnt/Cfdp1 that
109 cannot be ignored. Recently, we overcame the issue of off-target bands and assigned the
110 Western blotting signals of mouse Bcnt/Cfdp1 using a Cfdp1-K1 cell extract as a potential
111 negative control [33, 37]. In light of these findings, herein, we investigate the intracellular
112 trafficking of endogenous Bcnt/Cfdp1 in the mouse myoblast cell line C2C12, a well-
113 established model of myocyte differentiation and multinucleated myotube formation, and in
114 HEK293T cells. We also discuss the causes of the conflicting results regarding the subcellular
115 distribution of Bcnt/Cfdp1 between different approaches, considering nuclear export trafficking
116 and macromolecular crowding. Furthermore, we address the Bcnt/Cfdp1 function in the Srcap-C
117 framework.

118 **RESULTS**

119 **Observation of Bcnt/Cfdp1 in the Nucleus via Cytochemical Approaches**

120 Assessing the subcellular trafficking of the target molecule is essential for clarifying its
121 functional framework, and examining the endogenous ones is imperative. However, no reliable
122 antibodies against Bcnt/Cfdp1 are currently available for immunocytochemistry. Previously, we
123 detected tag-free mouse Bcnt/Cfdp1 primarily in the nuclei of human HEK293T cells by
124 immunocytochemistry with two antibodies generated against two peptides of mouse
125 Bcnt/Cfdp1: one is specific to mice and located in the N-terminal region and the other is
126 common to mice and humans in the C-terminus (Figure 1A, modified from Nakashima *et al.*
127 [37]).
128 Here, we used the myoblast C2C12 cell line, a well-known model of myocyte differentiation
129 and multinucleated myotube formation, to analyze the dynamic behavior of Bcnt/Cfdp1 during
130 these processes. We expressed N-terminal FLAG- and fluorescent protein-tagged mouse
131 Bcnt/Cfdp1 (mCherry or enhanced green fluorescent protein (EGFP)) in C2C12 cells. We
132 examined its subcellular distribution using immunostaining with an anti-FLAG antibody. The
133 experimental results showed that, while the control fluorescent multiple cloning site (MCS) was
134 distributed throughout the cell, the fluorescent protein-tagged Bcnt/Cfdp1 was predominantly
135 localized in the nuclei (Figure 1B-1).

136 The density of the nuclear interior is recognized as a porous medium composed of the chromatin
137 network [6]. The chromatin density is heterogeneous; the inactive part, heterochromatin, is
138 denser, whereas the active part, euchromatin, is sparser. Using high-resolution imaging, we
139 observed mCherry Bcnt/Cfdp1 and DAPI in the nucleus of C2C12 myoblasts and found their
140 segregation pattern; mCherry Bcnt/Cfdp1 was present in the area with weaker DAPI signals
141 (Figure 1B-2).
142 To gain insights into the intranuclear dynamics of Bcnt/Cfdp1, we examined its potential
143 involvement in forming the condensates in the nucleus using the N-terminal BCNT/CFDP1
144 IDR. Nevertheless, the results were in vain (Supplementary Figure 1S, which will be discussed
145 later). Furthermore, the fluorescent protein-tagged Bcnt/Cfdp1 remained stable during
146 prolonged culture, and multiple signals were visible in the nuclei (Figure 1C). These results
147 indicated that fluorescent protein-tagged Bcnt/Cfdp1 was detected primarily in the nuclei of
148 C2C12 myoblasts and differentiated multinucleated myotubes.

149 **Validity/Invalidity of Western Blot Monitoring in C2C12 Cell Subcellular Fractionation**
150 To determine the subcellular distribution of endogenous Bcnt/Cfdp1 in cells, we investigated
151 Bcnt/Cfdp1 through the biochemical fractionation of C2C12 and HEK 293T cells, monitored by
152 Western blot analysis, followed by mass spectrometry. Our previous study demonstrated that
153 the Western blotting signal of Bcnt/Cfdp1 corresponds to a doublet of ~43 kDa (previously
154 described ~45 kDa) bands in mouse ES cell lines Cfdp1-K1 and mouse brain extracts using
155 A305-624A-M as an anti-CFDP1 antibody [37]. We confirmed that the ~43 kDa signal band
156 represents Bcnt/Cfdp1 by enriching the immunoreactive band from Cfdp1-K1 cells using two-
157 column chromatography followed by mass spectrometry (Supplementary Figure S2 and
158 Supplementary Table S1). Next, we validated the Western blot signal(s) of C2C12 myoblast
159 extracts obtained with A305-624A-M (Figure 2A-D). The treatment of an endonuclease-derived
160 siRNA (esiRNA) against mouse *Bcnt/Cfdp1* significantly decreased the signal of the ~43 kDa
161 band, but the effects on the lower-mobility band(s) were lesser (Figure 2B and 2C). To confirm
162 whether the lower-mobility band is derived from Bcnt/Cfdp1, which was previously referred to
163 as the "upper band" corresponding to its phosphorylated form [10, 33], we expressed and
164 isolated FLAG-tagged mouse Bcnt/Cfdp1 in C2C12 cells (Figure 2D and Supplementary Figure
165 S3). A small upper band appeared in C2C12 cells expressing FLAG-tagged Bcnt/Cfdp1, but its
166 phosphorylated peptide at serine 245 in the ~43 kDa band [33] was not captured (data not
167 shown). These results conclude that the upper band exists, but its signal region contains both
168 Bcnt/Cfdp1-derived molecule and off-target(s), which will be discussed later.
169 Compared to the cytoplasmic soluble fraction, the particulate fraction exhibited several off-
170 targets unaffected by esiRNA treatment (Figure 2C). In addition, during myotube

171 differentiation, the distinct 50 kDa signal gradually increased, whereas Bcnt/Cfdp1 levels
172 decreased in the later stages (Figure 2E and Supplementary Figure S4). These results indicate
173 that Bcnt/Cfdp1 can be effectively monitored in the cytoplasmic soluble fraction of C2C12
174 myoblasts by Western blotting. However, tracking the target in the nuclear fraction and
175 differentiated cell extracts, including the upper band(s), may not be feasible. Consequently, we
176 focused on the cytoplasmic soluble fraction.
177
178 **Distribution of Bcnt/Cfdp1 by Subcellular Fractionation**
179 We performed biochemical fractionation using a widely utilized kit from Thermo Scientific,
180 which may include different detergents in each step [38]. C2C12 or HEK293T cell suspensions
181 were serially fractionated according to the manufacturer's protocol, with additional washes at
182 each step. The five resulting fractions were subjected to Western blotting analysis using
183 antibodies against Rasa1 (p120 Ras GTPase activating protein) and Gapdh (glyceraldehyde-3-
184 phosphate dehydrogenase) as markers of the cytoplasmic extract, Vdac1 (voltage-dependent
185 anion channel 1) for the membrane extract, NonO (non-POU domain-containing octamer-bound
186 p54nrb) for the soluble nuclear extract, and HstH3 (histone H3) as a marker of the chromatin-
187 bound fraction. Nestin, a linker protein that interacts with the cytoskeleton, was also used and
188 detected in the cytoskeletal fraction of C2C12 cells and the cytoplasmic fraction of HEK293T
189 cells (Figure 3). Under these fractionation conditions, a substantial amount of the ~43 kDa band
190 was detected in the cytoplasmic fraction, while the nuclear fraction contained other bands (s) of
191 ~50 kDa (Figure 4A). We subjected these five fractions of C2C12 myoblasts to quantitative
192 mass spectrometry to evaluate the fractionated preparations quantitatively. A total of 4,487
193 proteins were identified, of which 3,280 were eligible to evaluate relative distribution
194 (Supplementary Table S2). These included five biomarkers (Figure 4B), heterogeneous nuclear
195 ribonucleoproteins, and three paraspeckle proteins (Figure 4C). In sequential fractionation, the
196 components from the previous fractions were easily carried over into the following fraction.
197 Nevertheless, a significant amount of Bcnt/Cfdp1 was extracted in the first fraction, the
198 cytoplasmic fraction (Figures 4A and 4B). These results indicated that Bcnt/Cfdp1 is primarily
199 present in the cytoplasmic fraction of C2C12 cells using an available biochemical subcellular
200 fractionation kit and suggested that this is also the case for HEK293T cells (Figure 3, right
201 panel).
202 However, this result was in contrast to the above finding that the Bcnt/Cfdp1 was predominantly
203 observed in the nucleus using fluorescent protein labeling and immunocytochemical techniques
204 (Figures 1A–C). To gain insight into this intracellular Bcnt/Cfdp1 mobility during the
205 subcellular fractionation processes in C2C12 cells, we searched for proteins that showed similar
206 distribution to Bcnt/Cfdp1; the proteins annotated or reported to be present predominantly in the

207 nucleus are primarily detected in the cytoplasmic fraction. Of the 3,280 proteins available for
208 quantitative evaluation, 472 showed high relative occupancy (>0.6) in the cytoplasmic fraction,
209 of which six proteins were annotated as present in the nucleus (Figure 4D). They were IDR-
210 containing proteins, such as PEST proteolytic signal-containing nuclear protein, Pcnp [39].
211 Based on further curation using the integrated cellular localization prediction software BUSCA
212 [40] and experimental evidence from human ortholog data [41], these proteins may localize to
213 the cytoplasm (Supplementary Table S3).
214
215 **Intracellular Behavior of Bcnt/Cfdp1 in Digitonin-Mediated Release**
216 To further investigate the cytoplasmic distribution of Bcnt/Cfdp1 strictly, C2C12 and HEK293T
217 cell cultures on dishes were directly treated with digitonin to obtain the cytoplasmic soluble
218 proteins. Digitonin is a unique detergent that selectively binds to the cholesterol in membranes,
219 creating pores in cholesterol-rich membranes that allow macromolecules to pass through [42].
220 In addition, it has been observed that digitonin does not flip across membranes with low
221 cholesterol content, such as the nuclear envelope [43]. Therefore, digitonin is currently one of
222 the most appropriate methods for isolating the cytosolic proteins of mammalian cells while
223 exerting minimal effects on the intracellular behavior of other proteins, provided that the
224 treatment conditions are appropriately determined.
225
226 **A) In an isotonic solution**
227 C2C12 myoblasts on the dish were exposed to isotonic solutions containing different
228 concentrations of digitonin. The released eluate and corresponding residual cell contents were
229 collected and subjected to Western blotting analysis. A prominent band of ~43 kDa was
230 observed in the eluate at a digitonin concentration of 25 μg/mL, showing a similar pattern to
231 that of the cytoplasmic soluble proteins Rasa1 and Gapdh (Figure 5A). The ~43 kDa band was
232 excised from the gel and subjected to mass spectrometry analysis (Figure 5B). The data showed
233 that Bcnt/Cfdp1 was ranked high in the Sum Pep Score of 124 identified proteins annotated as
234 cytoplasmic proteins except for nuclear protein Trip13 (Supplementary Table S4 and Figure
235 5C). However, the human ortholog TRIP13 has been reported to be distributed diffusely in the
236 cytoplasm, in addition to the nucleus [44]. Thus, these results support the cytoplasmic
237 distribution of Bcnt/Cfdp1 in C2C12 myoblasts.
238 Furthermore, we developed a three-step strategy to enhance the collection of cytoplasmic
239 components, as shown in Figure 6. The supernatant released from the digitonin-treated cells was
240 initially collected, centrifuged, and labeled Cyt#1. Subsequently, the cell debris on the dish was
241 gently scraped off, and the supernatant was collected by centrifugation (Cyt#2). Next, the
242 supernatant was obtained by washing the pellet with an isotonic solution (Cyt#3). Following the

243 concentration of each fraction using trichloroacetic acid (TCA), the proteins were dissolved in
244 sodium dodecyl sulfate (SDS)-containing buffer. Equal relative volumes of each fraction were
245 subjected to Western blotting analysis, as shown in Figure 3. The elution pattern of Bcnt/Cfdp1
246 was similar to that of the cytoplasmic soluble marker proteins, such as Rasa1 and Gapdh (Figure
247 5D).
248
249 **B) In Ficoll/sucrose solution**
250 Macromolecular crowding has been shown to affect protein properties in living cells [2, 45],
251 nuclear structure and function in preparation [46], and subcellular distribution in subcellular
252 fractionation [47]. Therefore, digitonin treatment was performed in the HEPES-buffered
253 Ficoll/sucrose solution (HFS) instead of an isotonic solution to prepare the cytoplasmic
254 components from the cells appropriately. Cyt#1–3 fractions were prepared using the above
255 three-step process (Figure 6) and subjected to Western blotting analysis. Notably, the elution
256 pattern of Bcnt/Cfdp1 differed from that of the cytoplasmic soluble marker proteins (Figure
257 7A). A significant quantity of Bcnt/Cfdp1 was detected within the Cyt#3 fraction, whereas only
258 a tiny amount was observed within the Cyt#1 and #2 fractions at lower digitonin concentrations.
259 A comparative preparation was conducted using direct digitonin-mediated release in the HFS
260 solution on HEK293T cells grown on polylysine-coated dishes (Figure 7B). The distribution
261 pattern of BCNT/CFDP1 in HEK293T cells was similar to that observed in C2C12 cells. A
262 significantly higher concentration of BCNT/CFDP1 was also observed in the Cyt#3 fraction
263 than in the Cyt#1 and #2 fractions (Figure 7A). These results indicated that macromolecular
264 crowding affects the mobility of Bcnt/Cfdp1 in C2C12 and HEK293T cells during the three-step
265 preparation, suggesting that Bcnt/Cfdp1 exhibits flexible behavior in the process.
266

267 **Mobility of Bcnt/Cfdp1 in the Cytoplasm**
268 We expected that the differential elution pattern of digitonin-mediated release in the HFS
269 solution would reflect the mobility or integrity of each protein in the above three-step
270 preparation. To examine the perspective of the property, we prepared Cyt#1 and #2* similarly to
271 Figure 7, except that the pellet of Cyt#2 was washed with HFS solution instead of isotonic
272 solution, and the washed supernatant was combined and designated as Cyt#2* (Figure 8A).
273 These two fractions were subjected to quantitative LC-MS/MS analysis, and 2472 proteins were
274 identified, of which 2442 were qualified for ratio evaluation (Supplementary Table S5). Among
275 them, 51 glycolysis/glucogenesis- and TCA-related enzymes were listed, and their Cyt#1 to
276 Cyt#2* ratios (Cyt#1/2*) were plotted as LOG2 (Figure 8 B and C, and Supplementary Table
277 S6). The ratios of glycolysis-related proteins were above 1 (>0 in LOG2 unit), but TCA cycle-

278 or membrane-associated proteins had ratios significantly below 1 (< 0 in LOG2), while the
279 Bcnt/Cfdp1 ratio was 0.17 (-2.55 in LOG2) (Supplementary Table S5). Remarkably, the four
280 isoenzymes of cytoplasmic and mitochondrial types revealed clear property trends.

281 Table 1. Ct#1/2* ratios of four representative glycolysis/TCA-related isomers

Protein Names	Gene Symbol (Alias)	Intracellular localization	Mw (kDa)	Cyt#1/2* (Ratios)	Cyt#1/2*(LOG2)
Bucentaur/Craniofacial development protein1	Bcnt/Cfdp1 (cp27)		33.4	0.17	-2.56
Aconitase	Aco1	cytoplasmic	99	2.27	1.18
	Aco2	mitochondrial	85.4	0.072	-3.80
Enolase	Eno1	cytoplasmic	47.1	2.36	1.24
	Eno2	mitochondrial	37.2	0.055	-4.18
	Eno3	cytoplasmic	56.1	2.33	1.22
Aspartate aminotransferase	Got1	cytoplasmic	46.2	2.41	1.27
	Got2	mitochondrial	47.4	0.03	-5.06
Malate dehydrogenase	Mdh1	cytoplasmic	40	1.835	0.88
	Mdh2	mitochondrial	35.6	0.038	-4.72

282

283 Cyt#1 and 2* were prepared from the digitonin-mediated cytoplasmic fractions of C2C12 cells using
284 a three-step process, as shown in Figure 6. Each fraction was analyzed by quantitative mass spectroscopy.
285 The Cyt#1/2* ratios of three representative isomers were listed and compared.

286

287 Furthermore, the ratios Cyt#1/2* of 321 RNA-binding proteins selected based on published data
288 were significantly smaller than that of the entire population (p-value <0.01) (Figure 8C and
289 Supplementary Table S7). These results support the differential elution patterns of each protein
290 and reflect the mobility or integrity of each protein during the three-step preparation, which is
291 affected by macromolecular crowding.

292 **DISCUSSION**

293 Although the lack of high-quality anti-Bcnt/Cfdp1 antibodies made the analysis difficult in this
294 study, reliable data were obtained by quantitative mass spectrometry. Nuclear fractions and
295 extracts of differentiated myotubes of C2C12 cells showed several off-target bands of Western
296 blots using A305-624A-M as the anti-CFDP1 antibody [33], which is currently considered the
297 most reliable antibody in our Western blot analysis. These difficulties forced us to focus on the
298 cytoplasmic soluble proteins, which did not allow us to take advantage of the characteristics of
299 C2C12 cells. In this study, cytochemical approaches showed that Bcnt/Cfdp1 was mainly
300 observed in the nucleus, whereas biochemical fractionation detected the molecule at high levels
301 in the cytoplasmic fraction. Here, we discuss these contradictory results from the viewpoints of
302 nuclear export trafficking and macromolecular crowding and also address the potential
303 functionality of Bcnt/Cfdp1 in the Srcap-C chromatin frame.

304

305 **Bcnt/Cfdp1 Subcellular Distribution Determined by Cytochemical Approaches**

306 As reported in a previous study, we showed that tag-free mouse Bcnt/Cfdp1 is predominantly
307 localized in the nuclei of human HEK293T cells using antibodies against mouse Bcnt/Cfdp1
308 peptides (Figure 1A, modified from Nakashima *et al*. [37]). This strategy was excellent, but
309 these antibodies react with off-targets in Western blotting in HEK293T and C2C12 cells.
310 Therefore, we used FLAG- and fluorescent protein-tagged Bcnt/Cfdp1 to assess its subcellular
311 localization. The results showed that the signal was predominantly observed in the nuclei of
312 C2C12 myoblasts and differentiated myotubes (Figure 1B-1 and 1C). Furthermore, using
313 higher-resolution imaging in myoblast, Bcnt/Cfdp1 was detected in a segregated pattern, the
314 regions with the lower DAPI staining (Figure 1B-2). The result is consistent with the
315 observation that the *Drosophila* homolog YETI has been mapped to multiple sites on the
316 euchromatic region on salivary gland polytene chromosomes [11].

317 When SRCAP-C is prepared at a higher-salt extraction buffer such as 300 mM KCl,
318 BCNT/CFDP1 is scarcely captured as its component among other subunits [13, 48], which is, in
319 part, why Bcnt/Cfdp1 has often been neglected [11]. However, a recent study revealed that
320 BCNT/CFDP1 was significantly recovered when a lower-salt extraction buffer (150 mM NaCl)
321 was used for isolation from the reconstituted system composed of recombinant proteins
322 (personal communication, Dr. Shinya Watanabe, University of Massachusetts Medical School).
323 This finding suggests that either weak ionic interactions are critical for BCNT/CFDP1 to be a
324 component of the SRCAP-C or that high salt concentrations disrupt the specific environment,
325 such as a condensate, in which Bcnt/Cfdp1 is incorporated into SRCAP-C. The N-terminal
326 peptide of SWC5 was shown to have a potential for condensate formation through molecular
327 dynamics simulations [49]. Although the amino acid sequence of the N-terminal regions is quite
328 different between SWC5 and BCNT/CFDP1, both are IDRs rich in negatively and positively
329 charged amino acid residues. Thus, we explored the possibility of condensate formation of
330 BCNT/CFDP1 in the nucleus. The IDR of BCNT/CFD1 (the N-terminal 273 of 299 whole
331 amino acids) was inserted into an optoDroplet assay vector containing a nuclear localization
332 signal, and condensate formation was monitored [50] (Supplementary Figure S1). However, no
333 positive results were obtained.

334 Considering the findings of the higher-resolution imaging in which Bcnt/Cfdp1 is detected in
335 the lower chromatin density regions and the fact that the interchromatin is a porous medium [6],
336 Bcnt/Cfdp1 may dynamically behave in the nucleus for coupling with Srcap-C. Further insights
337 into the physical properties of Bcnt/Cfdp1 are expected in the context of weak ionic interactions
338 in Srcap-C formation.

339 Nonetheless, considerable concerns remain with respect to the cytochemical results. First, we
340 could not correctly evaluate the weak fluorescent signals in the cytoplasm, which were observed
341 at the level of fluorescence microscopy. However, it was challenging to visualize after
342 paraformaldehyde (PFA) fixation and subsequent anti-FLAG antibody detection, which are used
343 to minimize artifact signals. Therefore, to accurately evaluate these weak signals, considering
344 the side effects of exogenous protein expression, improvements in fixation and visualization
345 methods, including expression systems that can control gene copy numbers, are necessary.
346 Second, the fluorescent protein tag, corresponding to a mass of approximately 27 kDa, may
347 inhibit passive nuclear export [8], resulting in overestimating Bcnt/Cfdp1 nuclear localization.
348 Thus, it remains essential to prepare higher-quality anti-Bcnt/Cfdp1 antibodies.

349

350 **Effectiveness and Limitations of Western Blotting Monitoring**

351 We employed A305-624A-M as an anti-Bcnt/Cfdp1 antibody to effectively monitor the ~43
352 kDa band in Western blotting. The presence of Bcnt/Cfdp1 molecules in the ~43 kDa region
353 was confirmed by enrichment followed by mass spectrometry (Supplementary Figure S2 and
354 Supplementary Table S1). However, in contrast to the cytoplasmic soluble proteins, the
355 particulates and the extract of differentiated C2C12 myotubes showed several off-target bands
356 in the wide range of ~ 50 kDa (Figures 2C, 4, and 8). We reported similar bands in the
357 precipitate fraction of T-Rex cell extracts solubilized in Radio-Immunoprecipitation Assay
358 (RIPA) buffer (Supplementary Figure S4 in Iwashita *et al*. [33]). During myotube
359 differentiation, another signal of ~ 50 kDa gradually increased, whereas Bcnt/Cfdp1 levels
360 decreased in the later stages (Figure 2E and Supplementary Figure S3). The latter was consistent
361 with mRNA expression levels [51] (courtesy of Dr. Yan Fei Gao). Concerning the ~43 kDa
362 doublets, which are caused by phosphorylation in T-Rex cells (a HEK293 cell derivative) at the
363 250th serine residue of BCNT/CFDP1 [10] or the 245th serine residue of mouse Bcnt/Cfdp1
364 [33], its intensity in C2C12 cells was too weak to be accurately assessed. Taking these results
365 together, we focused on their cytosolic extracts without mentioning the doublets.

366

367 **Subcellular Fractionation Using the Available Fractionation Kit**

368 We first performed subcellular fractionation using a Thermo Scientific kit containing multiple
369 non-ionic detergents in each step [38]. Using the process, significant bands of 43–45 kDa were
370 observed in the cytoplasmic fractions of both C2C12 and HEK293T cells, and other bands of
371 ~50 kDa were detected in the respective nuclear fractions (Figure 3). The presence of
372 Bcnt/Cfdp1 in the cytoplasmic fraction was confirmed via mass spectrometry (Figure 5C from
373 Supplementary Table S2). Non-ionic detergents are often combined with a hypotonic solution to

374 achieve optimal results in sequential subcellular fractionation and have been reported to be
375 particularly effective in separating the cytoplasmic and nuclear compartments [52]. However,
376 the possibility that non-ionic detergents, even at low concentrations, affect lipid-lipid and lipid-
377 protein interactions, affecting the membrane-associated population of the targets and
378 compromising membrane integrity cannot be ignored.
379 The nucleus is protected by a fibrous layer called the lamina, which lies beneath the nuclear
380 envelope [53]. Therefore, the apparent intactness of the nucleus after various treatments does
381 not necessarily guarantee the integrity of the nuclear envelope. The nuclear membrane is much
382 more elastic than previously thought. Its integrity, even its rupture, is influenced by a
383 physiological response [54] and through signaling pathways, such as the activation of Akt
384 kinase [55]. Regarding the distribution of Bcnt/Cfdp1, it is interesting that HMGB1 was
385 detected in the cytoplasm using the non-ionic detergent IGEPAL (Nonidet P-40), but in the
386 nucleus using the Dounce homogenization method in lung cancer cell lines [56]. The
387 discrepancy may be attributed to the properties of HMGB1 that include nuclear localization
388 signals in the N-terminal and IDRs in the C-terminal. Notably, blocking the nuclear localization
389 signals of HMGB1 in leucocytes redirects it to the cytoplasm, eventually leading to secretion
390 [57]. In our mass analysis, Hmgb1 was mainly detected in the cytoplasmic fraction in the
391 subcellular fractionation of C2C12 and annotated in most compartments, including the non-
392 structural extracellular matrix (Supplementary Table S2). HMGB1, found initially as a nuclear
393 protein, may have properties similar to those of Bcnt/Cfdp1 in flexible intracellular behavior.
394 Regarding the possibility of Bcnt/Cfdp1 secretion, it was reported as an unconventionally
395 secreted protein in the conditioned medium of C2C12 myotubes [58]. Furthermore, a secretome
396 prediction tool supported the result: OutCyte, http://www.outcyte.com/(courtesy of Dr. Gereon
397 Poschmann) [59]. Although we tried to confirm the possibility, obtaining the C2C12 cell culture
398 medium supernatant was difficult even in myoblast cultures, as dead cells constituted at least
399 1% of the total. Thus, it was impossible to reach a definitive conclusion, and further research is
400 needed.
401
402 **Digitonin-Mediated Extraction in Isotonic or Ficoll/Sucrose Solution**
403 To examine Bcnt/Cfdp1 in the cytoplasm more strictly, we directly prepared the cytoplasmic
404 soluble proteins from cell cultures on the dishes by digitonin treatment. The method was
405 expected to allow the extraction of cytosolic proteins with minimal interference from other
406 proteins. In the experiment, Bcnt/Cfdp1 was detected along with the cytoplasmic soluble
407 proteins Rasa1 and Gapdh in isotonic buffer at a concentration of 25 μg/mL (0.0025%) (Figure
408 5A and Supplementary Table S4). Notably, a nuclear protein, Trip13 (thyroid hormone receptor
409 interactor 13), was released with the digitonin treatment and showed similar mobility to

410 Bcnt/Cfdp1 (Supplementary Table S2 and S4). Indeed, the human ortholog TRIP13 has been
411 reported to be significant trafficking in the cytoplasm and the nucleus [44]. These results
412 support the cytoplasmic distribution of Bcnt/Cfdp1 and the specific proteins that exhibit similar
413 molecular mobility. On the other hand, it was difficult to obtain reproducible release patterns at
414 lower digitonin concentrations because of the tailing of cytoplasmic soluble marker proteins
415 under the direct elution method, especially in the HFS solution.
416 Since macromolecular crowding is critical for molecular behavior [2, 45], we referred to the
417 following reports to examine the subcellular behavior and distribution of Bcnt/Cfdp1. First,
418 solutions without macromolecular crowding may not fully preserve the nuclear structure and
419 function during nuclear isolation [46], and second, the intracellular trafficking of SIRT1 may
420 depend on macromolecular crowding [47]. Therefore, according to the report, we used the HFS
421 solution instead of an isotonic solution in the digitonin treatment [47].
422 Notably, Bcnt/Cfdp1 was distinctly extracted compared to the cytoplasmic soluble proteins,
423 especially Rasa1, appearing in the Cyt#3 fraction rather than in the Cyt #1 and Cyt #2 fractions
424 (Figure 7). Cyt#3 was the supernatant fraction obtained by scraping the digitonin-treated cell
425 debris and washing the pellet with an isotonic solution, followed by centrifugation (Figure 6). A
426 comparable extraction pattern was also observed at a higher digitonin concentration of 250
427 μg/mL in C2C12 cells and 50 μg/mL in HEK293T cells.
428 We prepared the fractions of Cyt#1 and Cyt#2*, the latter obtained by washing the pellet of
429 Cyt#2 with HFS solution and combining the washed supernatant (Figure 8). The mass analysis
430 of Cyt#1 to #2* of ratios reflected the mobility of each protein in the cytoplasm. The ratio of
431 Bcnt/Cfdp1 was 0.17 (-2.55 in LOG2), suggesting that Bcnt/Cfdp1 exists in a complex in the
432 cytoplasm, probably associated with RNA or RNA-binding proteins [28]. This result reflects an
433 essentially similar phenomenon, as reported; the subcellular distribution of SIRT1 differs
434 depending on whether the fractionation solution is composed of macromolecular densities [47].
435 Although the rate at which the nuclear membrane is partially damaged, resulting in leakage out
436 of the nucleus during the three-step preparation, should not be underestimated, we propose that
437 Bcnt/Cfdp1 and some specific proteins have physical properties that allow them to be readily
438 mobile from the nucleus to the cytoplasm, which is affected by macromolecular crowding.
439 These findings have practical implications for future research and applications in protein
440 behavior.
441
442 **Beyond the Limitations of Digitonin Treatment -Conflicting Results for the Subcellular**
443 **Localization of Bcnt/Cfdp1**
444 The discrepancy in the subcellular distribution of Bcnt/Cfdp1 described above is a complex and
445 vital issue that presents significant challenges. As mentioned earlier, several factors could lead

446 to discrepancy. Two situations lead to overestimating nuclear localization: the cytochemical
447 approach could not capture the weak signals in the cytoplasm, and the fluorescent protein tag
448 could inhibit passive nuclear export. On the other hand, mobility due to nuclear membrane
449 damage in the digitonin-mediated preparation could lead to the overestimation of cytoplasmic
450 localization.

451 It was challenging to completely recover the cytoplasmic soluble proteins released by direct
452 digitonin treatment, especially in an HFS solution. Subsequently, we developed a three-step
453 strategy for the preparation of digitonin-mediated extracts. The Cyt#3 fraction obtained by
454 washing the digitonin-mediated cell debris pellet contains the proteins of the residual
455 cytoplasmic population, which may include the attached one to various organelle membranes. In
456 addition, proteins present in the nucleus may leak out of the nucleus due to damage to the
457 nuclear membrane during the three-step procedure. However, given the relatively selective
458 activity of digitonin in membrane poration, which depends on the cell type and physiological
459 state, it is inherently challenging to avoid partial membrane damage during digitonin treatment
460 to harvest the cytoplasmic components completely. For example, although digitonin treatment
461 can be mild, i.e., using 0.001% in phosphate-buffered saline (PBS) for 2 min on ice, it still
462 caused partial damage to the nuclear envelope, as evidenced by staining with an anti-lamin B1
463 Ab [60]. In addition, digitonin is capable of disordering the alkyl chains of phospholipid
464 monolayers, and its effect is more potent on phosphatidylethanolamine and phosphatidylserine
465 than phosphatidylcholine [61]. Orre *et al***.** performed a large-scale analysis of subcellular
466 localization in five cancer cell lines using a uniform fractionation method that involved the
467 digitonin treatment of cell cultures on dishes, followed by homogenization in a hypotonic buffer
468 [41]. Whereas the data showed 80% agreement between the cell lines, significant discrepancies
469 were attributed to the differences in the localization of proteins, including BCNT/CFDP1,
470 between the cytosol and nucleus (https://lehtio-lab.se/subcellbarcode/). This discrepancy might
471 be due to the different susceptibility of the nuclear envelope in some cells than in others during
472 the fractionation or due to other factors, such as differences in the levels of post-translational
473 phosphorylation in each cell. Furthermore, the unique intracellular mobility that we observed on
474 Bcnt/Cfdp1 and some proteins may also contribute similarly.
475 Beyond these difficulties of evaluation in digitonin-mediated preparation, our data suggest that
476 Bcnt/Cfdp1 and some proteins are readily mobile from the nucleus. Recent studies have
477 revealed unique features for the nuclear membrane compared to other cell membranes; nuclear
478 lipid membranes are much more elastic than other membranes [62], and their lipid composition
479 is closely related to membrane integrity [63]. Additionally, NPC, the sole transport gateway
480 between the cytoplasm and nucleus, comprises approximately 300 IDPs, rendering the pore a

481 flexible rather than a rigid structure. Interestingly, while folded protein transport has revealed a
482 size-dependent exclusion, where larger proteins are restricted, IDPs can diffuse through the
483 NPC without energy or specific transport receptors due to their lack of a fixed structure,
484 allowing them to navigate the pores more efficiently [9]. These results support the possibility
485 that Bcnt/Cfdp1 and some specific proteins may be able to diffuse rapidly through the NPC into
486 the cytoplasm during the subcellular fractionation. However, leakage due to partial damage to
487 the nuclear envelope cannot be underestimated in the three-step processes.
488

489 **Biological Functionality of Bcnt/Cfdp1**

490 *Bcnt/Cfdp1* plays a pivotal role in developmental processes, as evidenced by its mutants in
491 *Drosophila* [20], zebrafish [21, 22], and mice [23, https://www.jax.org/strain/033834]. These
492 biological variations include alterations to the cell cycle, cell migration, and apoptosis, which
493 subsequently influence cancer prognosis and susceptibility [28, 29].
494 The zebrafish mutant *gazami*, lacking the seventh exon of Bcnt/Cfdp1 (encoding the C-terminal
495 31 amino acid residues), exhibited abnormal neuronal differentiation in brain granule cells. The
496 elevated expression levels of cyclin B1 (*Ccnb1*) have been shown to contribute to inappropriate
497 differentiation [21]. However, its upregulation might be one of the gene expression variations
498 induced by deficient *cfdp1*, similar to the *Bcnt/Cfdp1* knocked down in the Cfdp1-K1 cells [33].
499 Interestingly, many genes related to the Wnt or Akt pathways and apoptosis/autophagy, such as
500 *Wls*, *Wnt4*, *Anxa2*, *Bcl2*, and *Akt2,* are included, up- or downregulated in Cfdp1-K1 cells
501 (Supplementary Table S8). They are involved in cell cycle control, cell migration, and
502 apoptosis. Indeed, the Wnt signaling pathway is suppressed specifically in extraluminal
503 mesenchymal cells of the valves of zebrafish Bcnt/Cfdp1-deficient embryos [22].
504 The broad effects of deficient *Bcnt/Cfdp1* may be comparable to natural genetic variations in the
505 fission yeast *swc5*. The mutant exhibited abnormal mRNA, antisense, and noncoding RNA
506 expression, possibly caused by improper histone exchange reactions [34]. Srcap-C has been
507 demonstrated to be involved in differentiation processes in intestinal epithelial cells controlled
508 by H2A.Z in association with Wnt signaling [64]. Assuming that Bcnt/Cfdp1, similarly to
509 SWC5 in SWR1-C, is a key factor for Srcap-C activity [14-16], a deficiency in ***Bcnt/Cfdp1*** may
510 induce inappropriate histone exchange reaction activity, resulting in changes to the
511 transcriptional landscape by Srcap-C. The phenotype of the mutant *gazami* described above may
512 be a clear example.
513 Notably, some reports of the biological responses of perturbed *BCNT/CFDP1* mentioned earlier
514 are partially associated with *BCAR1***,** a proximal neighboring gene of *BCNT/CFDP1* located on
515 chromosome 16q23.1 and has multiple functions [65]. The *BCAR1–CFDP1–TMEM170A* locus,

516 which is highly conserved across vertebrates, contains several single nucleotide polymorphisms
517 (SNPs) associated with diseases, such as vascular diseases [66] and Dupuytren's disease [67].
518 Although these diseases may be highly related to variations in the Wnt/Notch/Akt signaling
519 pathways, the causal relationship between these SNPs and diseases remains unclear.
520

521 **CONCLUSION**

522 Metazoan Bcnt/Cfdp1 is predicted to have a similar function to yeast SWC5 as a component of
523 Srcap-C. Consistent with this prediction, both untagged mouse Bcnt/Cfdp1 transfected into
524 HEK293T cells and fluorescent protein-tagged mouse Bcnt/Cfdp1 in C2C12 cells were detected
525 primarily in the nucleus by cytochemical approaches. However, by detergent-based biochemical
526 fractionation of C2C12 and HEK293T cells, endogenous Bcnt/Cfdp1 was detected mainly in the
527 cytoplasmic fraction. Furthermore, when cell cultures on the dish were treated with digitonin,
528 Bcnt/Cfdp1 was released and detected as a cytoplasmic protein, while different elution patterns
529 were observed between isotonic and Ficoll/sucrose solutions. Although our results on the
530 intracellular behavior of Bcnt/Cfdp1 reveal its mobility in the presence of detergent rather than
531 the export trafficking, we argue that Bcnt/Cfdp1 and some specific proteins have physical
532 properties that allow them to be readily mobile from the nucleus to the cytoplasm, which is
533 affected by macromolecular crowding. The unique property of Bcnt/Cfdp1 intracellular mobility
534 remains unclear, but its elastic properties at the cytoplasm/nucleoplasm interface may be
535 relevant. These issues are the most critical aspects of this study and are expected to become
536 more evident as our understanding of the nuclear membrane expands beyond classical cell
537 membrane studies [68].

538

539 **Data Availability Statement**

540 All data reported in this paper, including the proteomics mass spec dataset, are available without
541 restriction.

542

543 **MATERIALS AND METHODS**

544 Supplementary Table S9 provides detailed information on the material resources used in the
545 study, except for some experiments mentioned therein.

546 **Cell Culture**

547 C2C12 cells were obtained from the European Collection of Authenticated Cell Cultures
548 through KAC Co., Ltd. (Kyoto), expanded, and aliquots were stored at –80°C using Bambanker.
549 HEK293T cells were provided by Dr. Rie Komori (Tokushima Bunri University) and stored in
550 liquid nitrogen using Cellbanker. Both types of cells were cultured in Dulbecco's Modified
551 Eagle's Medium (DMEM)–10% FCS and subcultured using Accutase, as described previously
552 [33]. Briefly, after incubation for 5 min at room temperature, the cells were gently homogenized
553 using a 1000 μL tip, mixed with medium, centrifuged, and resuspended in the medium unless
554 otherwise specified. The cell numbers were counted using a hemocytometer (a disposable cell
555 counting plate of the Improved Neubauer Type), and dead cells were estimated via the trypan
556 blue exclusion assay. Before seeding, the dishes were incubated with the medium in a CO_2
557 incubator for at least 30 min.

558 **C2C12 Differentiation**

559 C2C12 cells (5 x 10^4 per 35 mm dish) were cultured for 2 days, and then the medium was
560 replaced with DMEM–2% horse serum (designated as day 0). On the corresponding day, the
561 cultures were washed with chilled HEPES buffered saline (HBS) twice and homogenized in 100
562 μL Lysis buffer (LS:1% SDS, 1 mM EDTA in 10 mM HEPES–NaOH, pH 7.5) supplemented
563 with inhibitors of proteases and phosphatases using a silicon policeman. Each extract was
564 collected in a 1.5 ml tube, boiled immediately for 3 min, and then sonicated for 2.5 min. A
565 constant volume of each extract was subjected to 12.5% SDS-polyacrylamide gel
566 electrophoresis (SDS/PAGE), followed by Western blot analysis.

567 **Coating Culture Dishes with Polylysine**

568 According to the protocol, 60 mm dishes were coated with polylysine with some modifications
569 (https://assets.thermofisher.com/TFS-Assets/BID/Flyers/gibco-poly-d-lysine-flyer.pdf). Each
570 dish was shaken with 1 mL of 50 μg/mL poly-d-lysine solution on a seesaw shaker for 1 h at
571 room temperature. To examine fluorescent protein-tagged mBcnt/Cfdp1, a commercially
572 available 4-well polylysine-coated chamber (Matsunami, Osaka) was used.

573 **Construction of Plasmids**

574 All Polymerase Chain Reaction (PCR) primers are listed in Supplementary Table S10. Tag-free
575 and FLAG-tagged Bcnt/Cfdp1 were generated as previously described [37]. The same primers
576 were used to generate mCherry- and EGFP-tagged MCS or mouse Bcnt/Cfdp1 using their
577 respective expression vectors (NCBI accession numbers LC311025, LC311020, LC311024, and
578 LC311019).

579 **Transfection of Plasmids**

580 Transfections were carried out using Lipofectamine 3000 according to the manufacturer's
581 protocol with minor modifications. Prior to transfection, each half of the medium was saved
582 once, and the plasmids were transfected. After 4 h, the saved medium was returned, and the
583 cells were cultured for 20-44 h. For the fluorescent protein observation, C2C12 cells were
584 seeded at a density of 1×10^4 cells per well in 0.75 mL medium per well of polylysine-coated
585 chamber, which was pre-incubated with culture medium in a CO_2 incubator. After 20 h
586 culturing, the medium was replaced with 0.5 mL of antibiotic-free medium, and cells were
587 transfected with 0.25 μg of each plasmid using Lipofectamine 3000 at a DNA-to-Lipofectamine
588 ratio of 1:2. Following 4 h of culture, 0.5 mL of medium containing 20% FCS was added to
589 each well. The cells were then cultured for an additional 20 h.

590 **Fluorescent Proteins by Immunocytochemistry**

591 The transfected and further cultured cells were washed twice with cold HBS and fixed with a
592 final concentration of 4% PFA by dilution in 0.1 M phosphate buffer (pH 7.2). The cells were
593 washed with 10 mM PBS to remove PFA. All the blocking serum, antibodies, and nuclear
594 staining dye were used at the indicated dilutions with 10 mM PBS containing 0.2% Triton X-
595 100. The cells were blocked with 5% normal donkey serum for 30 min at room temperature,
596 then incubated with the anti-DYKDDDDK tag monoclonal Ab (1:1000) at 4°C overnight. The
597 immunoreactivity was visualized with Cy3-conjugated donkey anti-mouse IgG (1:200) or
598 CF™488A-conjugated donkey anti-mouse IgG (1:200). DAPI (1 μg/mL) was used for nuclear
599 staining. The immunostained cells were examined by phase contrast and fluorescence
600 microscopy (TE2000-U, Nikon).

601 **Enrichment of ~43 kDa Band by Western Blot Monitoring**

602 A puromycin-resistant cell line of AB2.2 mouse embryonic stem cells was gifted from Dr.
603 Tsutomu Kumazaki (Tokushima Bunri University), who obtained the original AB2.2 cells from
604 the Sanger Institute (Cambridge, UK) and generated the cell line by transfection with
605 pMSCVpuro plasmid using PolyFect. The cells were expanded under serum- and feeder-layer-
606 free culture conditions as described in [33] without G418 and puromycin. The cells were
607 harvested using Accutase and rinsed with chilled HBS. The cell suspension aliquots were snap-
608 frozen in liquid nitrogen and stored at −80°C until use. For the experiment, the cell suspension
609 (equivalent to 3×10^7 cells) was thawed and resuspended in 300 μL of Solution 1 (a cytoplasmic
610 extraction buffer from Atto, Tokyo). The suspension was homogenized in a Biomasher II,
611 rotating the pestle 10 times, sonicated in an ice-water bath (10 s, three times), and then
612 centrifuged at 25,000 × *g* for 30 min at 4°C. Subsequently, CHAPSO ($C_{32}H_{58}N_2O_8S$) was added

613 to the supernatant at a final concentration of 1% (w/v). The extracts were slowly loaded onto
614 heparin-agarose (200 μL bed volume in a spin column) by cycling three times after the resin had
615 been equilibrated with Solution 1. Nonidet-P40 was included in all buffers at a final
616 concentration of 0.05% v/v, which was utilized for the subsequent chromatographic procedures.
617 After washing the resin with 20 mM Tris-NaOH, pH 7.5, the bound proteins were eluted twice
618 with 200 μL of Tris buffer containing different concentrations of NaCl. Each elution was
619 allowed 5 min to settle at each elution step. The eluates from the heparin column
620 chromatography with 0.05–0.1 M NaCl were combined and loaded onto Phos-tag resin (150-μL
621 volume in a spin column) by three cycles. The resin was washed thrice with 150 μL of wash
622 buffer, followed by a buffer containing 1M NaCl. The bound proteins were released using 4 ×
623 100 μL of phosphate-containing elution buffer without Nonidet-P40 following the
624 manufacturer's protocol (https://labchem-
625 wako.fujifilm.com/jp/category/docs/01072_doc01.pdf). The eluates were concentrated by
626 deoxycholate-TCA precipitation, as described in a standard protocol
627 (https://www.sigmaaldrich.cn/deepweb/assets/sigmaaldrich/product/documents/132/021/protprb
628 ul.pdf). One aliquot of preparation was stored in a buffer designed for two-dimensional gel
629 electrophoresis (Solution 2 from Atto Corp.). Following SDS/PAGE separation, the gel was
630 stained in silver staining, and a gel piece in the range of ~43 kDa was excised for mass
631 spectroscopy analysis.

632 **Subcellular Fractionation using Available Fractionation Kit**

633 C2C12 or HEK293T cells were harvested using Accutase, washed with DMEM-1% polyvinyl
634 alcohol (PVA), and then washed with chilled PBS. Cells were fractionated according to the
635 manufacturer's protocol, with modifications to minimize the contamination for the next step
636 (Thermo Fisher Scientific, https://assets.thermofisher.com/TFS-
637 Assets/LSG/manuals/MAN0011667_Subcellular_Protein_Fraction_CulturedCells_UG.pdf).
638 The samples were centrifuged, and the resulting supernatant was combined with the original
639 solution. The nuclear extraction buffer without $CaCl_2$ and nuclease was used for washing for
640 chromatin-bound nuclear fractionation. Each fraction was concentrated by TCA precipitation, as
641 described below. The resulting pellets were then dissolved in LS buffer and added to
642 concentrated SDS/PAGE sample buffer at a final concentration of 1 x boiled for 3 min. Finally,
643 equal relative volumes of each fraction were subjected to Western blotting analysis. To evaluate
644 the resulting five fractions, Rasa1 and Gapdh were used as marker proteins for the cytoplasmic
645 fraction, Vdac1 for the membrane fraction, NonO for the soluble nuclear fraction, and Histone
646 H3 for the chromatin-bound fraction. For quantitative mass spectrometry analysis, C2C12 cells
647 were seeded at 1.7 x 10^6 per 100 mm dish x 4 and cultured for 23 h. Duplicate samples were

648 prepared independently in subsequent steps. The cells were rinsed twice with 10 mL of warm
649 HBS and treated with 2 mL of Accutase per 100 mm dish. The incubation was carried out at
650 room temperature for 10 min with gentle rocking on a seesaw shaker while rotating the cell dish
651 at 90 degrees per 2 min. The suspended cells were gently homogenized with a 1000 μL tip to
652 prepare a single-cell suspension, which was then collected in a 15 mL tube. The cell
653 suspensions were combined by washing the dishes twice with 2 mL of chilled DMEM-1% PVA
654 and centrifuged for 1 min at 4°C. The percentages of trypan-blue-positive cells in the two
655 groups were 1.8 and 2.2%, respectively. The cells were subjected to a subcellular fractionation
656 at 10^6 cells per 100 μL of cytoplasmic solution from the kit. Each subcellular fractionated
657 sample was concentrated with TCA, as described above.

658 **Preparation of Digitonin Solution**

659 A stock solution of digitonin was prepared by mixing 25 mg per mL of H_2O at ~80°C. The
660 solution was then aliquoted and stored at –30°C. Before usage, the thawed aliquot was briefly
661 sonicated, heated to ~60°C, cooled to room temperature, and diluted as needed.

662 **Digitonin-Mediated Release in Isotonic Solution from C2C12 Cells**

663 C2C12 cells (4 x 10^5 cells) were seeded in a 6-well dish and cultured in 2 mL DMEM–10%
664 FCS for 26 h. After two rinses with 2 mL of chilled HBS, the plates were transferred to a cold
665 room, and sample preparation was performed below 4°C. The residual buffer was wholly
666 removed with filter paper, and the cells were immersed in 0.5 mL of isotonic solution (HEPES–
667 KOH, pH 7.5, 150 mM KCl, 2 mM $MgCl_2$, 1 mM EGTA, 1 mM β-mercaptoethanol). The plate
668 was gently rocking on a seesaw shaker for 10 min. Each fluid was collected into a 1.5 mL tube
669 and centrifuged at 10,000 × *g* for 10 min at 4 °C. Concurrently, using a silicone policeman, each
670 corresponding remaining cell in a 6-well dish was lysed in 100 μL of LS buffer, which included
671 a cocktail of inhibitors against proteases and phosphatases. Extracts were collected into 1.5 mL
672 tubes using a 200 μL bore-type tip. After vortexing and boiling for 5 min, the samples were
673 sonicated for 2.5 min. Each sample was concentrated with TCA and dissolved in LS buffer
674 using a mixer for over 1 h (Tomy Digital Biology, Tokyo). Final samples were prepared by
675 mixing 2× SDS/PAGE sample buffer to adjust to 1 x.

676 **Subcellular Fractionation with Digitonin in a Three-Step Process**

677 C2C12 cells (3 x 10^5) or HEK293T cells (4 x 10^5 cells in the polylysine-coated dish) were
678 cultured in a 60 mm dish for 42–44 h. Washing was performed in the same way as described
679 earlier. The cells were immersed in 1 mL of digitonin-containing isotonic solution or HFS
680 solution (6.8% Ficoll, 0.27 M sucrose, 3 mM $CaCl_2$, 2 mM $MgCl_2$ in 20 mM HEPES–KOH,
681 pH7.5) and gently rocked for 10 min while rotating the cell dish at 90 degrees per min on a

682 seesaw shaker to ensure even distribution of the solution. The dishes were placed on ice, and the
683 supernatant fluid was collected in a 1.5 mL tube. The tube was centrifuged at 1000 × ***g,*** 10 min,
684 4°C, and the resulting supernatant was designated Cyt#1, while the pellets were examined as
685 debris. The remaining cell layer was gently scraped off into a 0.5 mL isotonic or HFS solution
686 without digitonin using a cell scraper, and the extract was collected into a 1.5 mL tube using a
687 bore-type 1000 μL tip. The sample was mixed by vortexing for 5 s at dial 8, left to settle for 15
688 min on ice, and then centrifuged at 1000 × *g* for 10 min at 4°C; the supernatant was saved as
689 Cyt#2. The pellet was then homogenized in 500 μL isotonic solution. The homogenates were
690 mixed by vortexing and gentle pipetting with a bore-type 1000 μL tip and left for 5 min on ice
691 before centrifugation at 3000 × ***g*** for 10 min at 4°C. The supernatant was saved as Cyt#3. The
692 pellets were resuspended in 150 μL of RIPA buffer (20 mM Tris-HCl, pH 7.5, 150 mM NaCl,
693 0.5% sodium deoxycholate, 1% Nonidet-P40, 1 mM EDTA) containing proteinase and
694 phosphatase inhibitors. In some experiments, the pellets were treated with 0.2% Nonidet-P40
695 and analyzed as an NP40 fraction before being dissolved in RIPA buffer. Subsequently, they
696 were sonicated in an ice-water bath for 2.5 min (10 s intervals, 15 times) and centrifuged at
697 25,000 × *g* for 30 min at 4°C. The supernatant was designated RIPA-Sup, while the pellets were
698 dissolved in 50 μL LS. They were vortexed, immediately boiled for 3 min, and analyzed as the
699 RIPA–Ppt fraction.
700
701 **Treatment with esiRNA**
702 C2C12 cells were seeded in a 24-well plate at 2 x 10^4 cells per well. After 20 h culture, the
703 medium was replaced with 300 μL of either regular medium (A group) or FCS-free DMEM (B
704 group). Four hours later, transfection was performed with 0, 50, or 100 nM of esiRNA targeting
705 mouse *Cfdp1* (Sigma-Aldrich, dissolved in 1 mM sodium citrate, pH 6.4) using Lipofectamine
706 3000. After 4 h, 300 μL of regular medium (to A group) or DMEM containing 20% FCS (to B
707 group) was added, and the cells were cultured for an additional 44 h. The cells were rinsed twice
708 with chilled HBS and scraped off using a silicone policeman in 50 μL of LS buffer
709 supplemented with inhibitors against proteases and phosphatases. The cell lysates were
710 harvested in a 1.5 mL tube and then boiled immediately. After sonication (10-s intervals x 10),
711 the samples were centrifuged at 25,000 × *g* for 30 min at 22°C. Constant amounts of protein (20
712 μg) were subjected to Western blot analysis. For examination of siRNA effects on subcellular
713 fractionation, C2C12 cells were seeded at a density of 5 x 10^4 or 1 x 10^5/35 mm dish and
714 cultured for 19 h, treated with esiRNA (0, 50, or 100 nM) using Lipofectamine for 44 h. The
715 digitonin-mediated fractionation was carried out in an HFS solution similar to the above three-
716 step process with the following modification. After obtaining the supernatant of Cyt#1 using 0.4
717 mL of an HFS solution containing 250 μg/ml digitonin, the residual cell layers were scraped off

718 in 0.2 mL of an HFS solution and centrifuged without vortexing. The pellets were suspended in
719 0.2 mL HFS solution with brief vortexing and standby for 15 min on ice, then centrifuged, and
720 the supernatant was combined as Cyt#2*. After washing the second pellets with HBS, the
721 pellets were resolved in LS buffer, and the fraction was designated as Particulate. Cyt#1 and
722 #2* were precipitated by TCA treatment, and the precipitates were resolved in 80 μL LS buffer.
723 Equal amounts of proteins in each fraction of Cyt#1 (15 μg), Cyt#2*(7 μg), and Particulate (25
724 μg) were subjected to Western blot analysis.

725 **Examination of Potential LLPS of BCNT/CFDP1 in the Nuclei**

726 Plasmid construction and optoDroplet assays were performed in the same way as previously
727 reported [50]. The IDR of BCNT/CFDP1 was estimated using the PONDR VSL2 algorithm
728 (http://www.pondr.com/). The IDR fragment of BCNT/CFDP1 (residues 1–273) was amplified
729 by PCR from a human cDNA library (generated from total RNA extracted from HEK293T
730 cells. Primers were described in Supplementary Table S10). An optoDroplet assay vector was
731 constructed from the Cry2 vector and mCherry using the NEBuilder HiFi DNA Assembly Kit to
732 incorporate the BCNT/CFDP1 fragment. HEK293T cells were transfected with the plasmids
733 using TurboFect, and potential LLPS activity was measured after 48 h by image monitoring
734 (Nikon Ti2 inverted microscope with the A1R confocal laser scanning system). After acquiring
735 background mCherry images, cells were imaged using blue light stimulation (488 nm
736 stimulation/3 s, interval/17 s, mCherry imaging/10 s x 3), followed by mCherry imaging
737 (imaging/10 s and interval/50 s x 10).

738 **Isolation of Transiently Expressed FLAG-tagged Bcnt/Cfdp1**

739 C2C12 cells (5 x 10^5 cells/100 mm dish) were cultured for 21 h, transfected with the F-
740 *Bcnt/Cfdp1* plasmid (10 μg), and cultured for an additional 42 h until they were nearly
741 confluent. The cells were rinsed twice with chilled HBS on ice and scraped off using a cell
742 scraper in 0.5 ml RIPA buffer containing inhibitors against proteinases and phosphatases. The
743 lysates were collected in a 1.5 mL tube, sonicated for 2.5 min (15 × 10-s pulses at 10-s
744 intervals), and centrifuged at 25,000 × *g* for 30 min at 4°C. The resulting supernatant was snap-
745 frozen in liquid nitrogen and stored at −80°C until use. The frozen extract was thawed,
746 sonicated in an ice-water bath (3 × 10-s pulses at 10-s intervals), and centrifuged at 10,000 × *g*
747 for 1 min at 4°C. The isolation of F-Bcnt/Cfdp1 was essentially the same as described
748 previously [33] except for using RIPA buffer to equilibrate the agarose before mixing the cell
749 extract.

750 **TCA Precipitation**

751 TCA precipitation was carried out according to a protocol with some modifications
752 (https://www.thermofisher.com/document-connect/document-
753 connect.html?url=https://assets.thermofisher.com/TFS-
754 Assets%2FLSG%2Fmanuals%2FMAN0011667_Subcellular_Protein_Fraction_CulturedCells_
755 UG.pdf). The pellets were washed once with acetone and twice with a 4:1 acetone/water
756 mixture. The samples were sonicated in an ice-water bath (10-s x 2) and centrifuged during each
757 washing step. Finally, the sample tubes were heated in a bath at ~95°C for 2 min to evaporate.

758 **Immunoblotting and Densitometric Analysis**

759 Immunoblotting was performed using SDS/PAGE on a 15% gel, followed by electroblotting
760 onto a polyvinylidene fluoride (PVDF) membrane, as previously described [33, 37]. The Abs
761 used in the experiments are listed in Supplementary Table S9. Immunoreactivity was detected
762 using horseradish peroxidase (HRP)-conjugated secondary Abs via a chemical fluorescent
763 method as previously described [33, 37]. For the subcellular fractionation assay, after
764 SDS/PAGE and transferred to a PVDF membrane, the membrane was briefly rinsed with water,
765 followed by Tris-buffered saline containing 0.1% Tween-20 (TBT), then wrapped in plastic
766 wrap and cut into three parts, higher than 75 kDa (upper), 75–25 kDa (middle), and below 25
767 kDa, using a cutter based on the position of the prestained SDS/PAGE standard molecular
768 weight markers. It was sometimes cut into four parts: higher than 75 kDa, 75–40 kDa, 40–20
769 kDa, and lower than 20 kDa. Each filter was blocked with 0.1 % skim milk in TBT for over 2 h
770 at room temperature and then incubated at 4°C overnight with Abs against Rasa 1 (upper),
771 CFDP1 (middle), and HstH3 (lower). The upper and middle membrane parts were subjected to
772 stripping, followed by blocking, and processed to access by Abs against nestin, NonO for a 75–
773 40 Da range membrane, and Vdac1 for a 40–25 or 40–20 kDa range membrane. Finally, the
774 middle or 40–20 kDa range membrane was stripped and then incubated with an HRP-
775 conjugated anti-Gapdh Ab after blocking. Multi-box strays were routinely used for all
776 incubation procedures of blocking, reaction with Abs, and washing (Ina Optika MWB-06 or
777 MWB-4). All images were captured at 5.51M Pixel via a GeneGNone-5 (Syngene Bio Imaging)
778 using GeneSnaps software and saved as tiff files. The densitometric evaluation of Western blot
779 signals was conducted using the Band/Peak Quantification plugin in Fiji software [69].

780 **Mass Spectroscopy Analysis**

781 The Coomassie brilliant blue (CBB)-stained bands or Western blot-positive bands in the ~43-
782 kDa range in the SDS/PAGE gel were excised and destained, and the samples were processed in
783 duplicate as previously described [10, 33, 37]. They were subjected to trypsin digestion and
784 subsequently analyzed using nano LC-MS/MS with a Q Exactive mass spectrometer. Each

785 sample was run in duplicate or triplicate for mass spectrometry analysis. In the study of the
786 subcellular fractionated samples, SDS/PAGE was performed, and electrophoresis was stopped
787 upon the entry of the samples into the separation gel to treat each as a single band. Each band
788 was excised and subjected to reductive acrylamidation. The samples were digested with trypsin,
789 and equal amounts of each were analyzed in triplicate using the Q Exactive HF-X. The data
790 were analyzed using Proteome Discoverer 3.0 and MASCOT server 2.8 for protein
791 identification and quantification (Supplementary Table S2). For examination of Cyt#1/#2*
792 ratios, each fraction precipitated with TCA was also subjected to brief SDS/PAGE as described
793 above. Each protein concentration was determined based on amino acid composition and
794 analyzed in triplicate. Data were acquired using the Proteome Discoverer 2.4 and MASCOT
795 server 2.7 (Supplementary Table S5). The data of Tables S2 and S5 are available via
796 ProteomeXchange with the identifier PXD063720
797 http://proteomecentral.proteomexchange.org/. The distribution of Cyt#1 to Cyt#2* ratios was
798 presented as violin plots, and their statistical analysis was performed using EZR [70]
799 (https://cran.r-project.org/web/packages/RcmdrPlugin.EZR/RcmdrPlugin.EZR.pdf).

800 **Figure Legends**

801 **Figure 1**
802 **Detection of Bcnt/Cfdp1 primarily in the nucleus by a cytochemical approach**

803 A cytochemical approach was employed to detect the localization of Bcnt/Cfdp1, primarily in
804 the nucleus.

805 **A. Use of tag-free mouse Bcnt/Cfdp1 in HEK293T cells**

806 HEK293T cells were cultured in dishes coated with polylysine, transfected with plasmids
807 encoding tag-free mouse Bcnt/Cfdp1 or unrelated proteins, and immunostained with an anti-
808 Bcnt-N Ab (a, b) or anti-Bcnt-Cter Ab (c, d). The image was visualized using Alexa488-
809 conjugated secondary Ab. The two Abs were generated against two peptides, respectively. The
810 N-terminal amino acid sequence of Bcnt/Cfdp1 was aligned with its human counterpart, with
811 red letters indicating different amino acids. The original images are published by Nakashima et
812 al. [36].

813 **B. Use of fluorescent protein-tagged mouse Bcnt/Cfdp1 in C2C12 myoblasts**

814 **B-1.** C2C12 cells were cultured in dishes coated with polylysine and transfected with plasmids
815 encoding EGFP-MCS (a, b) or EGFP-Bcnt/Cfdp1 (c, d). Following a 24 h incubation, the cells
816 were fixed with 4% PFA on ice. The samples were immunostained with anti-FLAG Ab
817 followed by CF488A conjugated secondary Ab. The nuclei were stained with DAPI (b, d). The

818 merged images of EGFP and DAPI on phase contrast pictures are shown (b, d). The scale bars
819 indicate 25 μm.

820 **B-2**. C2C12 myoblasts transfected with Flag-mCherry-Bcnt/Cfdp1, similarly cultured and
821 stained as Figure 1B-1, were observed at higher resolution using Leica Mica microscopy.
822 Bcnt/Cfdp1 was stained with anti-Flag Ab followed by Cy3-conjugated secondary Ab (b); the
823 nuclei were stained with DAPI (c), and the merged image of mCherry and DAPI is shown (a).
824 The scale bar indicates 10 μm.

825 **C. In differentiated C2C12 myotubes**

826 After 24 h of culturing the EGFP-MCS (a, b), EGFP-Bcnt/Cfdp1 (e, f, i, j), mCherry-MCS (c, d)
827 or mCherry-Bcnt/Cfdp1 (g, h, k, l) transfectants, the medium was replaced with differentiation
828 medium (DMEM containing 2% horse serum (DM)). The cells were cultured for an additional 4
829 days with daily DM changes, after which they were fixed with 4% PFA. The samples were
830 immunostained with an anti-FLAG Ab followed by CF488A- or Cy3-conjugated secondary Ab,
831 and the nuclei were stained with DAPI (b, d, f, h, j, l). The merged images of EGFP, mCherry,
832 and DAPI on phase contrast pictures are shown (b, d, f, h, j, l). Scale bars indicate 50 μm (a–h)
833 and 25 μm (i–l).

834 **Figure 2**
835 **Validity of Western blotting monitoring in C2C12 cell subcellular fractionation**

836 **A. Western blotting signals of Bcnt/Cfdp1 in C2C12 cells**

837 Extracts from whole C2C12 cells (equivalent to 7.5 x 10^4) or mouse embryo brains (15 μg) were
838 subjected to Western blotting analysis using A305-624A-M as an anti-Bcnt/Cfdp1 Ab.

839 **B. Effects of esiRNA knockdown of Bcnt/Cfdp1 in C2C12 cells.**

840 C2C12 cells were treated with 0, 50, or 100 nM esiRNA for 24 h. Each extract was prepared by
841 scraping off the cells in LS buffer and boiling. After centrifugation, equal amounts of protein
842 (20 μg) were subjected to Western blotting analysis. The upper and middle sections of the image
843 show Western blotting signals using Abs against Rasa1 and Bcnt/Cfdp1, respectively. The red
844 and blue arrows correspond to the target and upper band. At the bottom, densitometric analysis
845 of blots of Bcnt/Cfdp1 (red bar), "upper band(s)" (dark blue), and Rasa1 (light blue) are shown
846 as bar graphics with the mean ± SEM of duplicate experiments.

847 **C. Effects of esiRNA on the cytosolic and particulate proteins**

848 C2C12 cells were cultured in 35 mm dishes and treated with esiRNA (0 or 50 nM). Cytosolic
849 and particulate proteins were obtained using an HFS solution containing 250 μg/ml digitonin, as
850 detailed later in Figures 6-8. Briefly, digitonin-mediated released fluid was the cytosolic
851 fraction, and the particulates were obtained by scrapping off the remaining cell layer in HFS
852 solution followed by centrifugation. The cytosolic fraction was concentrated with TCA
853 precipitation followed by resuspending in LS buffer, while the particulate fraction was directly
854 resolved in LS buffer. Equal relative amounts of each fraction (approximately 15 or 25 μg of
855 protein, respectively) were subjected to Western blotting analysis to assess the degree of
856 separation using anti-histone H3 Ab in addition to that in Fig. 3B. The red and blue arrows
857 correspond to the target and "upper band," respectively. Asterisks (*) indicate off-target bands.

858 **D. The presence of the "upper band" in the FLAG-tagged Bcnt/Cfdp1**

859 C2C12 cells were transfected with F-MCS or F-Bcnt/Cfdp1 (Tf: transfection). After 24 h of
860 culture, one sample from each group was replaced with serum-free medium (St: serum-starved)
861 and cultured for 6 h. All cell cultures were harvested and subjected to Western blotting analysis
862 using anti-Bcnt/Cfdp1 (upper panel) or anti-FLAG (lower panel) Abs. The blue arrows indicate
863 the "upper band" of F-Bcnt/Cfdp1.

864 **E. The appearance of a cross-reacted 50 kDa band during C2C12 differentiation**

865 C2C12 cell cultures were switched from regular medium to DMEM containing 2% horse serum,
866 designated as day 0. Cell extracts were collected and subjected to Western blotting analysis the
867 following day. The red and blue arrows indicate Bcnt/Cfdp1 and an unrelated 50 kDa band. At
868 the bottom, densitometric analysis of blots of Bcnt/Cfdp1 (red bar) and 50 kDa band (dark blue)
869 are shown as bar graphics with the mean ± SEM of duplicate experiments.

870

871 **Figure 3**

872 **The presence of Bcnt/Cfdp1 in the cytoplasmic fraction determined using a widely used kit**

873 For subcellular fractionation of C2C12 or HEK293T cells, each cell suspension (1×10^6 cells)
874 was subjected to fractionation according to the manufacturer's protocol, which was slightly
875 modified with additional washes to minimize contamination at each step. Each fraction was
876 concentrated by TCA precipitation and resolved in LS buffer. To show the relative occupancy
877 of all fractions except WCE, equal volumes of each were subjected to Western blotting analysis.
878 The following proteins were accessed: Rasa1 (Ras GTPase activating protein 1), Gapdh
879 (glyceraldehyde-3-phosphate dehydrogenase), Vdac1 (voltage-gated anion channel 1), non-POU

880 domain-containing octamer-binding protein (NonO), HstH3 (histone H3), and Bcnt/Cfdp1 using
881 A305-624A-M. The asterisks in the signals detected with the anti-Bcnt/Cfdp1 Ab indicate the
882 off-target band. Abbreviations at the top of the figure. WCE: whole cell extract, Cyt:
883 cytoplasmic extract, Mem: membrane extract, s-N: soluble nuclear extract, c-N: chromatin-
884 bound nuclear extract, and Ppt: pellet extract.

885

886 **Figure 4**

887 **Quantitative analysis of the subcellular fractionated samples accessed by Western blotting**
888 **or by mass spectrometry**

889 **A.** Distribution of six marker proteins in each fraction accessed by Western blotting

890 Densitometric analysis of Western blots of six biomarker proteins (Bcnt/Cfdp1, Rasa 1,
891 Gapdh, Vdac1, NonO, and HstH3) in C2C12 subcellular fractions of Figure 3 is shown. Data
892 represent the relative occupancy of each marker protein in the five fractions, in which total
893 amounts are set as 1.0, and the bars represent the mean ± SEM of results obtained from five
894 independent experiments. Cyt, cytoplasmic fraction; Mem, membrane fraction; s-N, soluble
895 nuclear fraction; c-N, chromatin-bound fraction; Ppt, precipitates.

896 **B–D**

897 Two independent C2C12 myoblast cultures were fractionated in a manner analogous to that
898 described in Figure 4. Each fraction was subjected to quantitative mass spectrometry analysis. A
899 total of 4,489 proteins were identified, and the average abundance of each component was
900 calculated and displayed graphically. Cyt, cytoplasmic fraction; Mem, membrane fraction; s-N,
901 soluble nuclear fraction; c-N, chromatin-bound fraction; CSK, cytoskeleton.

902 **B.** Distribution of six marker proteins in each fraction accessed by mass analysis

903 Data represent the relative amounts of each marker protein per cell extract in the five fractions,
904 in which total amounts of Bcnt/Cfdp1 are set at 1.0, and bars represent the mean ± SEM of
905 results obtained from two independent experiments.

906 **C.** The intracellular distributions of three paraspeckle components and 18 heterogeneous
907 nuclear ribonucleoproteins

908 The data are shown in relative quantitative amounts, with the total Bcnt/Cfdp1 set at 1.0. The
909 data represent the means of two experiments.

910 **D.** The intracellular distribution of six proteins

911 The intracellular distribution of proteins screened as those detected in the cytoplasmic fraction
912 despite being annotated localized in the nucleus is shown. The relative distribution of each
913 protein is shown from the mean value of the two experiments.

914

915 **Figure 5**
916 **Release of Bcnt/Cfdp1 by digitonin treatment in an isotonic solution**

917 **A.** Cell cultures in 12-well dishes were exposed to a range of digitonin concentrations in an
918 isotonic solution for 10 min on a rocking shaker. After the supernatant of each eluate was
919 collected, the corresponding extracts of the residual cellular debris were scraped in an SDS-
920 containing buffer and boiled. Equal volumes of each sample were subjected to Western
921 blotting using Abs against Rasa1 (upper box), Bcnt/Cfdp1 (middle box), and Gapdh (lower
922 box). After Western blotting analysis, the membrane was stained with CBB to show the 37–
923 75 kDa region (at the bottom).
924 **B.** The eluate supernatant was subjected to SDS/PAGE, and after staining the gel with CBB, the
925 ~43 kDa region was excised for mass spectroscopic analysis.
926 **C.** After destaining the gel pieces, they were subjecting tryptic digests to liquid
927 chromatography-tandem mass spectrometry analysis. Of the 124 proteins identified
928 (Supplementary Table S4), data are shown for Bcnt/Cfdp1, with 41% recovered by the
929 analyzed fragments.
930 **D.** Using the three-step preparation of the digitonin-mediated eluate, as illustrated in Figure 7,
931 Cyt #1–3 fractions were obtained using digitonin at 125 μg/mL in an isotonic solution.
932 Following TCA precipitation, each pellet was dissolved in LS buffer (containing 1% SDS),
933 and relatively equal volumes of each fraction were subjected to Western blotting analysis, as
934 described in the legend of Figure 3. The dark blue arrow and asterisks correspond to the
935 "upper band" of Bcnt/Cfdp1 and probable off-target band(s). Densitometric analysis of the
936 Western blotting is shown at the bottom. The data represent the relative occupancy of each
937 of the six marker proteins in each fraction (Cyt#1–RIPA–Ppt), with the total amounts of
938 each marker protein set at 1.0.

939

940 **Figure 6**
941 **Schematic diagram of the three-step preparation of the digitonin-mediated eluates**

942 Cultured cells were immersed in an isotonic or HEPES/Ficoll/sucrose (HFS) solution containing
943 digitonin while the dish was rotated. The eluate supernatant was referred to as Cyt#1 after
944 centrifugation. The remaining cell debris was scraped off using a cell scraper in a digitonin-free
945 isotonic or HFS solution, and the supernatant was stored as Cyt#2 after centrifugation. The
946 pellet was washed by suspension in an isotonic solution, and the supernatant was stored as
947 Cyt#3 following centrifugation. The pellet was resuspended in RIPA buffer, sonicated, and
948 centrifuged. The supernatant was used as the RIPA fraction, the pellet was dissolved in SDS-
949 containing buffer, and the supernatant was analyzed as the Ppt fraction. In the case of isotonic
950 solution, the pellets were solved in 0.2% Nonidet-40. The details of the procedure are described
951 in the Materials and Methods section.

952

953 **Figure 7**

954 **Differential release of Bcnt/Cfdp1 from cytosolic proteins by digitonin treatment in HFS**

955 The Cyt#1–3 fractions were obtained using digitonin in HFS solution at 50 or 250 μg/mL in
956 C2C12 cells or 50 μg/mL in HEK293T cells, as illustrated in Figure 6. Following TCA
957 precipitation, each pellet was dissolved in LS buffer, and relatively equal volumes of each
958 fraction were subjected to Western blotting analysis, as described in the legend in Figure 3.
959 Densitometric analysis of the Western blotting is shown at the bottom. The data represent the
960 relative occupancy of each of the six marker proteins in each fraction (Cyt#1–RIPA–Ppt), with
961 the total amounts of each marker protein set at 1.0.

962

963 **Figure 8**

964 **Mobility or integrity of digitonin-mediated released proteins in the Cytoplasm -Evaluation**
965 **from the ratios of two fractions-**

966 **A.** C2C12 cells treated with esiRNA (0, 50, or 100 nM) were subjected to digitonin-mediated
967 fractionation in HFS solution at 250 μg/mL digitonin, as shown in Figure 6. But, after
968 obtaining Cyt#2, its pellet was washed with HFS solution but not with isotonic solution, and
969 the washed supernatant was combined to give Cyt#2*. Furthermore, the precipitate was
970 dissolved in LS buffer after washing with HBS as a Particulate fraction. Equal amounts of
971 protein from Cyt#1 (15 μg), Cyt#2* (7 mg), and Particulate (25 mg) fractions were
972 subjected to Western blot analysis. These different protein amounts were adjusted so that
973 the relative occupancy volumes of the three fractions were approximately equal. Each Cyt#1

974 and #2* fraction was subjected to quantitative mass spectrometry analysis (Supplementary
975 Table S5).
976 **B.** Fifty-one glycolysis/glucogenesis/TCA cycle/organelle-associated enzymes were listed
977 from the 2442 qualified proteins by quantitative mass analysis (Supplementary S6). Each
978 Cyt#1/2* ratio value is plotted on the vertical axis as LOG2, while the horizontal axis shows
979 its molecular weight (Mw). Glycolysis-related cytosolic proteins (magenta circles),
980 organelle-related proteins (Diverse, orange circles), and TCA-related mitochondrial proteins
981 (dark blue circles) are shown.
982 **C.** The distribution of Cyt#1/2* ratios of 51-enzymes shown in Figure 8B (magenta, orange,
983 dark blue), 2442 qualified total proteins (purple), and 321 RNA-binding proteins (green),
984 which are selected based on published data were presented (Supplementary Table S7) as
985 violin plots, respectively, using EZR software. The rectangles within the violin plots
986 indicate the first and third quartiles, with central + as mean values. Results of statistical
987 analysis are shown. ** indicates a significant difference with $P<0.01$

988

989 **Acknowledgments**

990 We thank Dr. Tsutomu Kumazaki for the puromycin-resistant AB2.2 cell line. We appreciate
991 Drs. Shinya Watanabe and Dimitris Beis for information on the properties of Bcnt/cfdp1. We
992 acknowledge Drs. Yan Fei Gao, Gereon Poschmann, Lauri A. Aaltonen, and Justin Cotney for
993 sharing unpublished data. We also thank the following scientists for their valuable insights
994 during this research: Drs. Satoshi Yoshitome, Yasuhiro Kashino, Atsushi Iwai, Masahiro
995 Nishibori, Naoyuki Kataoka, Richard Schulz, Heiko Heerklotz, Song-Tao Liu, Takuto Shimizu,
996 and Mitsuru Okuwaki. We were encouraged by Dr. Stephane Twigg for his comments regarding
997 the nomenclature of the CFDP1 gene. We are willing to thank Editage (www. editing. com) for
998 precision editing the manuscript. We were indebted to Professors Si-Young Song, Hiromi
999 Nochi, and Takashi Tominaga for their support and encouragement.

References

1. Antifeeva, I.A., Fonin, A.V., Fefilova, A.S., Stepanenko, O.V., Povarova, O.I., Silonov, S.A., et al. (2022) Liquid-liquid phase separation as an organizing principle of intracellular space: overview of the evolution of the cell compartmentalization concept. Cell Mol Life Sci. 79, 251. 10.1007/s00018-022-04276-4

2. Jalihal, A.P., Schmidt, A., Gao, G., Saffron, R., Little, S.R., Pitchiaya, S., et al. (2021) Hyperosmotic phase separation: Condensates beyond inclusions, granules and organelles. J Biol Chem. 296, 100044. 10.1074/jbc.REV120.010899

3. Watson, J.L., Seinkmane, E., Styles, C.T., Mihut, A., Krüger, L.K., McNally, K.E., et al. (2023) Macromolecular condensation buffers intracellular water potential. Nature 623, 842-852. 10.1038/s41586-023-06626-z

4. Zhao, Y.G., Zhang, H. (2020) Phase separation in membrane biology: The interplay between membrane-bound organelles and membraneless condensates. Dev Cell 55, 30-44. 10.1016/j.devcel.2020.06.033

5. Kim, T., Jaeyoon Yoo, J., Do, S., Hwang, D.S., YongKeun Park, Y.K. (2023) RNA-mediated demixing transition of low-density condensates. Nat Commun. 14, 2425. 10.1038/s41467-023-38118-z

6. Hertzog, M., Erdel, F. (2023) The material properties of the cell nucleus: A matter of scale. Cells 12, 1958. 10.3390/cells12151958

7. Hampoelz, B., Andres-Pons, A., Kastritis, P., Beck, M. (2019) Structure and assembly of the nuclear pore complex. Annu Rev Biophys. 48, 515-536. 10.1016/j.devcel.2020.06.033

8. Timney, B.L., Raveh, B., Mironska, R., Trivedi, J.M., Kim, S.J, Russel, D., et al. (2016) Simple rules for passive diffusion through the nuclear pore complex. J Cell Biol. 215, 57-76. 10.1016/j.devcel.2020.06.033

9. Junod, S.L., Kelich, J.M., Ma, J., Yang, W. (2020) Nucleocytoplasmic transport of intrinsically disordered proteins studied by high-speed super-resolution microscopy. Protein Sci. 29, 1459-1472. 10.1073/pnas.1914313117

10. Iwashita, S., Suzuki, T., Yasuda, T., Nakashima, K., Sakamoto, T., Kohno, T., et al. (2015) Mammalian Bcnt/Cfdp1, a potential epigenetic factor characterized by an acidic stretch

in the disordered N-terminal and Ser250 phosphorylation in the conserved C-terminal regions. Biosci Rep. 35, e00228. 10.1042/BSR20150111

11. Messina, G., Celauro, E., Atterrato, M.T, Giordano, E., Iwashita, S., Dimitri, P. (2015) The Bucentaur (BCNT) protein family: a long-neglected class of essential proteins required for chromatin/chromosome organization and function. Chromosoma 124, 153-162. 10.1007/s00412-014-0503-8

12. Yu, J., Sui, F., Gu, F., Li, W., Yu, Z., Wang, Q., et al. (2024) Structural insights into histone exchange by human SRCAP complex. Cell Discov. 10, 15. 10.1038/s41421-023-00640-1

13. Cai, Y., Jin, J., Florens, L., Swanson, S.K., Kusch, T., Li, B., et al. (2005) The mammalian YL1 protein is a shared subunit of the TRRAP/TIP60 histone acetyltransferase and SRCAP complexes. J Biol Chem. 280, 13665-13670. 10.1074/jbc.M500001200

14. Huang, Y., Sun, L., Pierrakeas, L., Dai, L., Pana, L., Luk, E., et al. (2020) Role of a DEF/Y motif in histone H2A-H2B recognition and nucleosome editing. Proc Natl Acad Sci U S A. 117, 3543-3550. 10.1073/pnas.1914313117

15. Jalal, A.S.B., Girvan, P., Chua, E. Y. D., Liu L., Wang, S., McCormack, E. A., et al. (2024) Stabilization of the hexasome intermediate during histone exchange by yeast SWR1 complex. Mol Cell 84, 3871-3884.e9. 10.1016/j.molcel.2024.08.015

16. Sun, L., Luk, E. (2017) Dual function of Swc5 in SWR remodeling ATPase activation and histone H2A eviction. Nucleic Acids Res. 45, 9931-9946. 10.1093/nar/gkx589

17. Ishida, H., Kono, H. (2022) Free energy landscape of H2A-H2B displacement from nucleosome. J Mol Biol. 434, 167707. 10.1016/j.jmb.2022.167707

18. Saccharomyces Genome Database. https://www.yeastgenome.org/

19. Morillo-Huesca, M., Clemente-Ruiz, M., Andújar, E., Prado, F. (2010) The SWR1 histone replacement complex causes genetic instability and genome-wide transcription misregulation in the absence of H2A.Z. PLoS One 5, e12143. 10.1371/journal.pone.0012143

20. Messina, G., Damia, E., Fanti, L., Atterrato, M.T., Celauro, E., Mariotti, F.R, et al. (2014) *Yeti*, an essential *Drosophila melanogaster* gene, encodes a protein required for chromatin organization. J Cell Sci. 127, 2577-2588. 10.1242/jcs.150243

21. Itoh, T., Inoue, S., Sun, X., Kusuda, R., Hibi, M., Shimizu, T. (2021) Cfdp1 controls the cell cycle and neural differentiation in the zebrafish cerebellum and retina. Dev Dyn. 250, 1618-1633. 10.1002/dvdy.371

22. Giardoglou, P., Deloukas, P., Dedoussis, G., Beis, D. (2023) *Cfdp1* Is Essential for Cardiac Development and Function. Cells 12, 1994. 10.3390/cells12151994

23. Ito, Y. (2012) CP27: Expression, Regulation, and Function of a Chromatin Complex Member (Doctoral dissertation, University of Illinois at Chicago)

24. Doolan, P., Barron, N., Kinsella, P., Clarke, C., Meleady, P., O'Sullivan, F., et al. (2012) Microarray expression profiling identifies genes regulating sustained cell specific productivity (S-Qp) in CHO K1 production cell lines. Biotechnol J. 7, 516-526. 10.1002/biot.201100255

25. Xu, L., He, Y., Ding, Y., Liu, G.E., Zhang, H., Cheng, H.H., et al. (2018) Genetic assessment of inbred chicken lines indicates genomic signatures of resistance to Marek's disease. J Anim Sci Biotechnol. 9, 65. 10.1186/s40104-018-0281-x

26. Messina, G., Atterrato, M.T., Prozzillo, Y., Piacentini, L., Losada, A., Dimitri, P. (2017) The human Cranio Facial Development Protein 1 (Cfdp1) gene encodes a protein required for the maintenance of higher-order chromatin organization. Sci Rep. 7, 45022. 10.1038/srep45022

27. Moustakas, A., Heldin, C.H. (2007) Signaling networks guiding epithelial-mesenchymal transitions during embryogenesis and cancer progression. Cancer Sci. 98, 1512-1520._ 10.1111/j.1349-7006.2007.00550.x

28. Ming, R., Li, X., Wang, E., Wei, J., Liu, B., Zhou, P., et al. (2022) The prognostic signature of head and neck squamous cell carcinoma constructed by immune-related RNA-binding proteins. Front Oncol. 12, 795781. 10.3389/fonc.2022.795781

29. Zhou, Y., Qiu, J., Liu, S., Wang, P., Ma, D., Zhang, G., et al. (2023) CFDP1 promotes hepatocellular carcinoma progression through activating NEDD4/PTEN/PI3K/AKT signaling pathway. Cancer Med. 12, 425-444. 10.1002/cam4.4919

30. Cuadrado, A., Corrado, N., Perdiguero, E., Lafarga, V., Muñoz-Canoves, P., Nebreda, A.R. (2010) Essential role of p18Hamlet/SRCAP-mediated histone H2A.Z chromatin incorporation in muscle differentiation. EMBO J. 29, 2014-2025. 10.1038/emboj.2010.85

31. Dong, S., Han, J., Chen, J., Liu, T., Huen, M.Y.S., Yang, Y. (2014) The human SRCAP chromatin remodeling complex promotes DNA-end resection. Curr Biol. 24, 2097-2110. 10.1016/j.cub.2014.07.081

32. Välimäki, N., Jokinen, V., Cajuso, T., Kuisma, H., Taira, A., Dagnaud, O., et al. (2023) Inherited mutations affecting the SRCAP complex are central in moderate-penetrance predisposition to uterine leiomyomas. Am J Hum Genet. 110, 460-474. 10.1016/j.ajhg.2023.01.009

33. Iwashita, S., Suzuki, T., Kiriyama, Y., Dohmae, N., Ohoka, Y., Song, S.Y., et al. (2020) Overcoming off-targets: assessing Western blot signals for Bcnt/Cfdp1, a tentative component of the chromatin remodeling complex. Biosci Rep. 40, BSR20194012. 10.1042/BSR20194012

34. Clement-Ziza, M., Marsellach, F., Codlin, S., Papadakis, M.A., Reinhardt, S., Rodríguez-López, M., et al. (2014) Natural genetic variation impacts expression levels of coding, non-coding, and antisense transcripts in fission yeast. Mol Syst Biol. 10, 764. 10.15252/msb.20145123

35. Hagting, A., Jackman, M., Simpson, K., Pines, J. (1999) Translocation of cyclin B1 to the nucleus at prophase requires a phosphorylation-dependent nuclear import signal, Curr Biol **9**,680-9. 10.1016/s0960-9822(99)80308-x.

36. Pinarbasi, E.S., Tolga Cağatay, T., Fung, H.Y.J., Li, Y.C., Chook, Y.M., Thomas, P.J. (2018) Active nuclear import and passive nuclear export are the primary determinants of TDP-43 localization. Sci Rep. 8, 7083. 10.1038/s41598-018-25008-4

37. Nakashima, K., Iwashita, S., Suzuki, T., Kato, C., Kohno, T., Kamei, Y., et al. (2019) A spatial similarity of stereochemical environments formed by amino acid residues defines a common epitope of two non-homologous proteins. Sci Rep. 9, 14818. 10.1038/s41598-019-51350-2

38. Ramsby, M.L., Makowski, G.S. (2005) Differential detergent fractionation of eukaryotic cells. In: Walker, J.M. (ed) The Proteomics Protocols Handbook. Springer Protocols Handbooks. Humana Press. 10.1385/1-59259-890-0:037

39. Afzal, A., Sarfraz, M., Li, G.L., Ji, S., Duan, S.F., Khan, N.H., et al. (2019) Taking a holistic view of PEST-containing nuclear protein (PCNP) in cancer biology. Cancer Med. 8, 6335-6343. 10.1002/cam4.2465

40. Savojardo, C., Martelli, P.L., Fariselli, P., Profiti, G., Casadio, R. (2018) BUSCA: an integrative web server to predict subcellular localization of proteins. Nucleic Acids Res. 46, W459–W466. 10.1093/nar/gky320

41. Orre, L.M., Vesterlund, M., Pan, Y., Arslan, T., Zhu, Y., Woodbridge, A.F., et al. (2019) SubCellBarCode: Proteome-wide mapping of protein localization and relocalization. Mol Cell 73, 166-182.e7. 10.1016/j.molcel.2018.11.035

42. Lorent, J.H., Quetin-Leclercq, J., Mingeot-Leclercq, M.P. (2014) The amphiphilic nature of saponins and their effects on artificial and biological membranes and potential consequences for red blood and cancer cells. Org Biomol Chem. 12, 8803-8822. 10.1039/C4OB01652A

43. Fan, H.Y., Heerklotz, H. (2017) Digitonin does not flip across cholesterol-poor membranes. J Colloid Interface Sci. 504, 283-293. 10.1016/j.jcis.2017.05.034

44. Wang, K., Sturt-Gillespie, B., Hittle, J.C., Macdonald, D., Chan, G.K., Yen, T.J., et al. (2014) Thyroid hormone receptor interacting protein 13 (TRIP13) AAA-ATPase is a novel mitotic checkpoint-silencing protein. J Biol Chem. 289, 23928-23937. 10.1074/jbc.M114.585315

45. Minton, A.P. (2006) How can biochemical reactions within cells differ from those in test tubes? J Cell Sci. 119, 2863-2869. 10.1242/jcs.03063

46. Hancock, R., Hadj-Sahraoui, Y. (2009) Isolation of cell nuclei using inert macromolecules to mimic the crowded cytoplasm. PLoS One 4, e7560. 10.1080/15384101.2016.1211214

47. Sun, L., Fang, J. (2016) Macromolecular crowding effect is critical for maintaining SIRT1's nuclear localization in cancer cells. Cell Cycle 15, 2647-2655. 10.1080/15384101.2016.1211214

48. Yu, J., Sui, F., Gu, F., Li, W., Yu, Z., Wang, Q., et al. (2024) Structural insights into histone exchange by human SRCAP complex. Cell Discov. 10, 15. 10.1038/s41421-023-00640-1

49. Chu, W.T., Wang, J. (2021) Thermodynamic and sequential characteristics of phase separation and droplet formation for an intrinsically disordered region/protein ensemble. PLoS Comput Biol. 17, e1008672. 10.1371/journal.pcbi.1008672

50. Shin, Y., Berry, J., Pannucci, N., Haataja, M.P., Toettcher, J.E., Brangwynne, C.P. (2017) Spatiotemporal control of intracellular phase transitions using light-activated optoDroplets. Cell 168, 159-171. 10.1016/j.cell.2016.11.054

51. Li, H.K., Zhou, Y., Ding, J., Xiong, L., Shi, Y.X., He, Y.J., et al. (2020) LRTM1 promotes the differentiation of myoblast cells by negatively regulating the FGFR1 signaling pathway. Exp Cell Res. 396, 112237. 10.1016/j.yexcr.2020.112237

52. Senichkin, V.V., Prokhorova, E.A., Zhivotovsky, B., Kopeina, G.S. (2021) Simple and efficient protocol for subcellular fractionation of normal and apoptotic cells. Cells 10, 852. 10.3390/cells10040852

53. Houben, F., Ramaekers, F.C.S., Snoeckx, L.H.E.H., Broers, J.L.V. (2007) Role of nuclear lamina-cytoskeleton interactions in the maintenance of cellular strength. Biochim Biophys Acta 1773, 675-686. 10.1016/j.bbamcr.2006.09.018

54. Gunn, A.L., Yashchenko, A.I., Dubrulle, J., Johnson, J., Hatch, E.M. (2024) A high-content screen reveals new regulators of nuclear membrane stability. Sci Rep. 14, 6013. 10.1038/s41598-024-56613-1

55. Fan, J.R., Chang, S.N., Chu, C.T., Chen, H.C. (2023) AKT2-mediated nuclear deformation leads to genome instability during epithelial-mesenchymal transition. iScience 26, 106992. 10.1016/j.isci.2023.106992

56. Herrmann, C., Avgousti, D.C., Weitzman, M.D. (2017) Differential salt fractionation of nuclei to analyze chromatin-associated proteins from cultured mammalian cells. Bio Protoc. 7, e2175. 10.21769/BioProtoc.2175

57. Youn, J.H., Shin, J.S. (2006) Nucleocytoplasmic shuttling of HMGB1 is regulated by phosphorylation that redirects it toward secretion[1]. **J Immunol.** 177, 7889-7897. 10.4049/jimmunol.177.11.7889

58. Cox, J., Jensen, L.J., Meissner, F., Mann, M. (2015) Secretome analysis of lipid-induced insulin resistance in skeletal muscle cells by a combined experimental and bioinformatics workflow. J Proteome Res. 14, 4885-4895. 10.1021/acs.jproteome.5b00720

59. Zhao, L., Poschmann, G., Waldera-Lupa, D., Rafiee, N., Kollmann, M., Stühler, K. (2019) OutCyte: a novel tool for predicting unconventional protein secretion. Sci Rep. 9, 19448.

10.1038/s41598-019-55351-z

60. Chien, H.M., He, R.Y., Lee, C.C., Huang, Y.A., Hung, I.J., Hou, K.T., et al. (2021) Nanoscopic investigation of C9orf72 poly-GA oligomers on nuclear membrane disruption by a photoinducible platform. Commun Chem. 4, 111. 10.1038/s42004-021-00547-6

61. Orczyk, M., Wojciechowski, K., Brezesinski, G. (2017) Disordering effects of digitonin on phospholipid monolayers. Langmuir 33, 3871-3881. 10.1021/acs.langmuir.6b04613

62. Dazzoni, R., Grélard, A., Morvan, E., Bouter, A., Applebee, C.J., Loquet, A. (2020) The unprecedented membrane deformation of the human nuclear envelope. in a magnetic field, indicates formation of nuclear membrane invaginations. *Sci Rep* **10**,5147. 10.1038/s41598-020-61746-0

63. Romanauska, A., Köhler A (2023) Lipid saturation controls nuclear envelope function. *Nat Cell Biol* **25**,1290-1302. 10.1038/s41556-023-01207-8

64. Rispal, J., Escaffit, F., Trouche, D. (2020) Chromatin dynamics in intestinal epithelial homeostasis: A paradigm of cell fate determination versus cell plasticity. Stem Cell Rev Rep. 16, 1062-1080. 10.1007/s12015-020-10055-0

65. Leal, M.P.C., Sciortino, M., Tornillo, G., Colombo, S., Defilippi, P., Cabodi, S. (2015) p130Cas/BCAR1 scaffold protein in tissue homeostasis and pathogenesis. Gene 562, 1-7. 10.1016/j.gene.2015.02.027

66. Nurnberg, S.T., Guerraty, M.A., Wirka, R.C., Rao, H.S., Pjanic, M., Norton, S., et al. (2020) Genomic profiling of human vascular cells identifies TWIST1 as a causal gene for common vascular diseases. PLoS Genet. 16, e1008538. 10.1371/journal.pgen.1008538

67. Riesmeijer, S.A., Kamali, Z., Ng, M., Drichel, D., Piersma, B., Becker, K., et al. (2024) A genome-wide association meta-analysis implicates Hedgehog and Notch signaling in Dupuytren's disease. Nat Commun. 15, 199. 10.1038/s41467-023-44451-0

68. Anand, D., Chaudhuri, A. (2023) Grease in the nucleus: Insights into the dynamic life of nuclear membranes. J Membr Biol. 256, 137-145. 10.1007/s00232-022-00272-8

69. Ohgane, K., Yoshioka, H. (2019) Quantification of gel bands by an Image J macro, band/peak quantification tool. Protocols.io. 10.17504/protocols.io.7vghn3w

70. Kanda, Y. (2013) Investigation of the freely available easy-to-use software 'EZR' for medical statistics. Bone Marrow Transplant 48, 452-458. 10.1038/bmt.2012.244

Footnote references

[‡]The official name of *Bcnt/Cfdp1* is *Cfdp**1***. However, genetic studies of disease (1) or transcriptome analysis (2) do not provide solid evidence for its involvement in craniofacial development, including tooth development (3). Therefore, the nomenclature of *Cfdp1* is misleading and may need to be more accurate. To maintain consistency with previous studies, the name *Bcnt/Cfdp1* is used instead of *Cfdp**1*** in this article.

1. Twigg, S.R.F., Wilkie, A.O.M. (2015) New insights into craniofacial malformations. Hum Mol Genet. 24, R50-R59. 10.1093/hmg/ddv228

2. Yankee, T.N., Oh, S., Winchester, E.W., Wilderman, A., Robinson, K., Gordon, T., et al. (2023) Integrative analysis of transcriptome dynamics during human craniofacial development identifies candidate disease genes. Nat Commun. 14, 4623. 10.1038/s41467-023-40363-1

3. Hallikas, O., Roy, R.D., Christensen, M.M., Renvoisé, E., Sulic, A.M., Jernvall, J. (2021) System-level analyses of keystone genes required for mammalian tooth development. J Exp Zool B Mol Dev Evol. 336, 7, 10.1002/jez.b.23009

Figure 1

Detection of Bcnt/Cfdp1 primarily in the nucleus by a cytochemical approach

A Use of tag-free mouse Bcnt/Cfdp1 in HEK293T cells

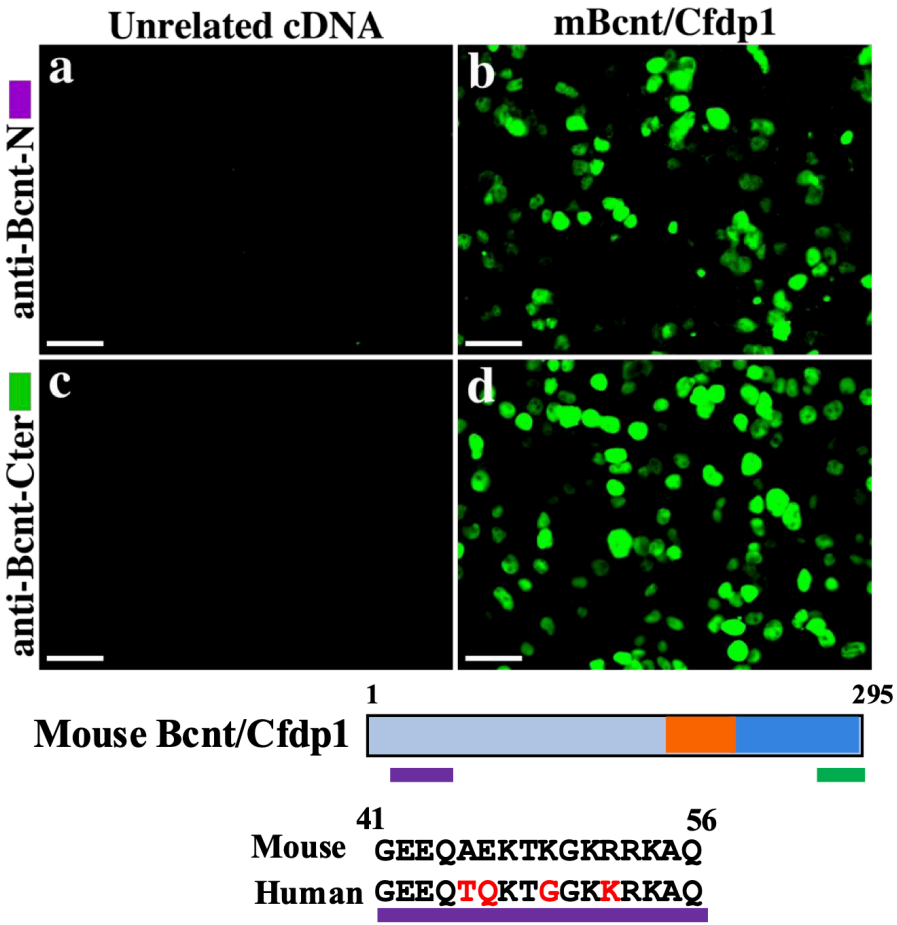

Figure 1B-1

Figure 1B-2

B **Use of fluorescent protein-tagged mouse Bcnt/Cfdp1 in C2C12 myoblasts**

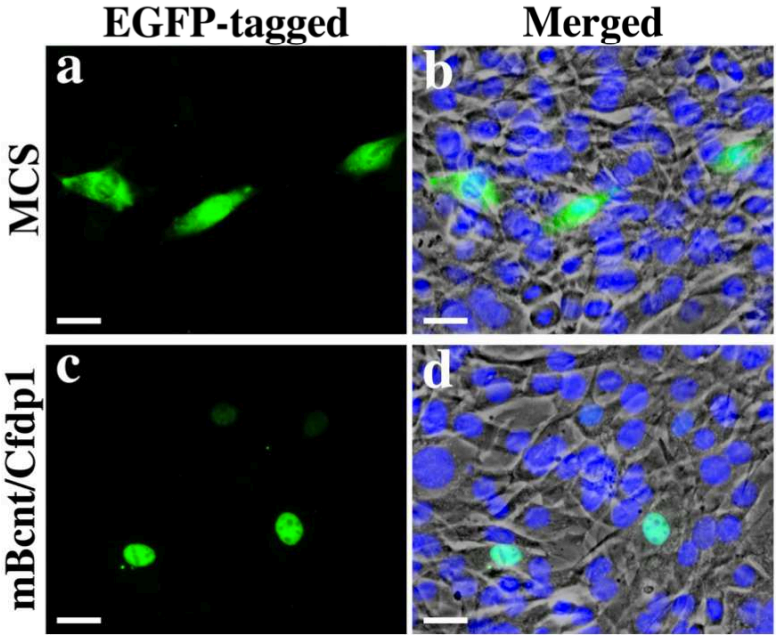

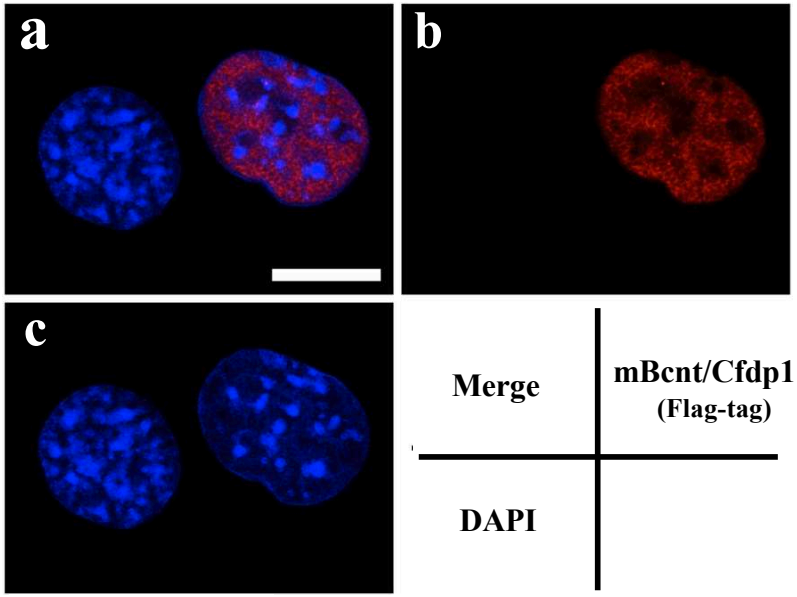

Figure 1C

C In differentiated C2C12 myotubes

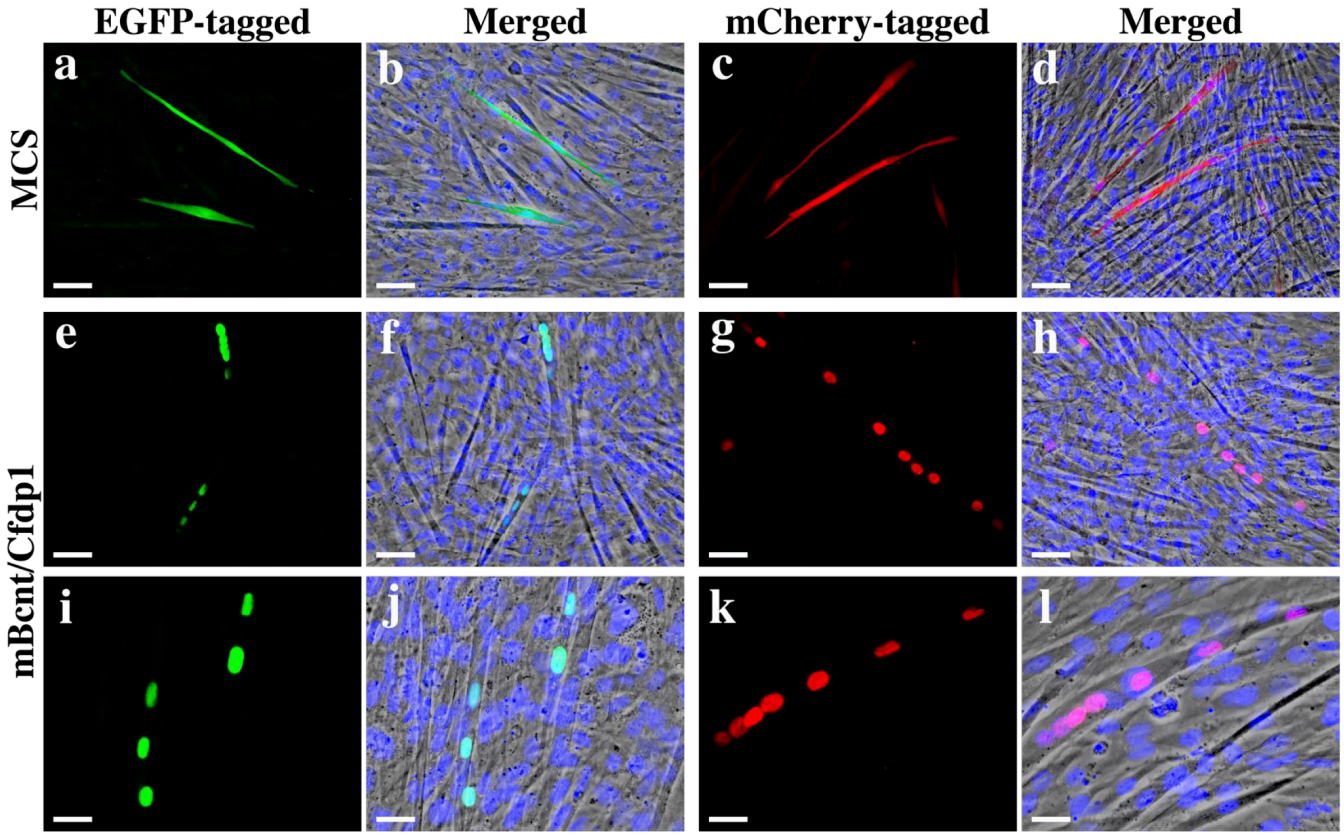

Figure 2

Validity of Western blotting monitoring in C2C12 cell subcellular fractionation

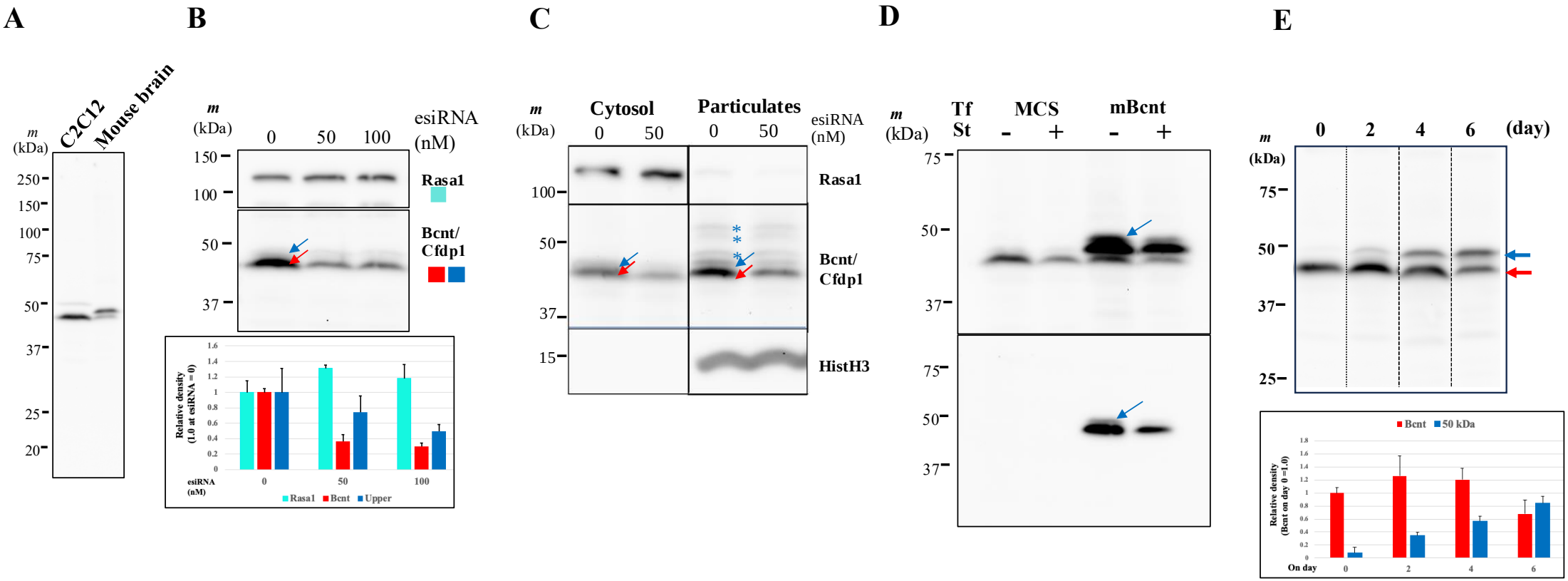

Figure 3

Presence of Bcnt/Cfdp1 in the cytoplasmic fraction determined using a widely used kit

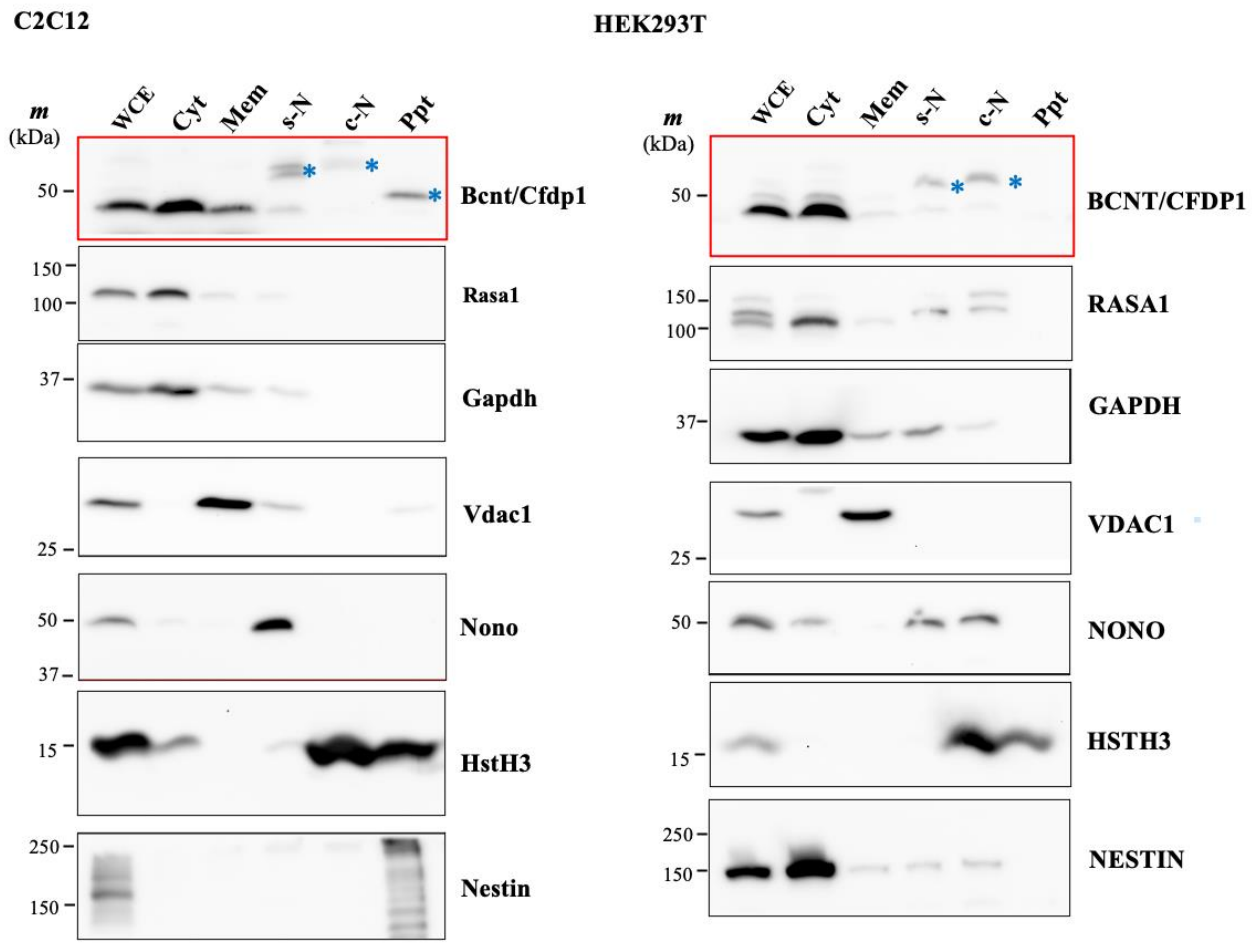

Figure 4

Quantitative analysis of subcellular fractionated samples

A

Marker proteins by Western blotting analysis

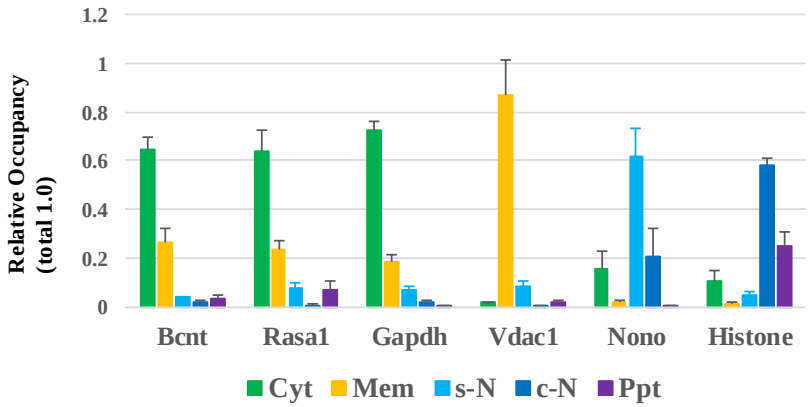

B

Marker proteins by Mass analysis

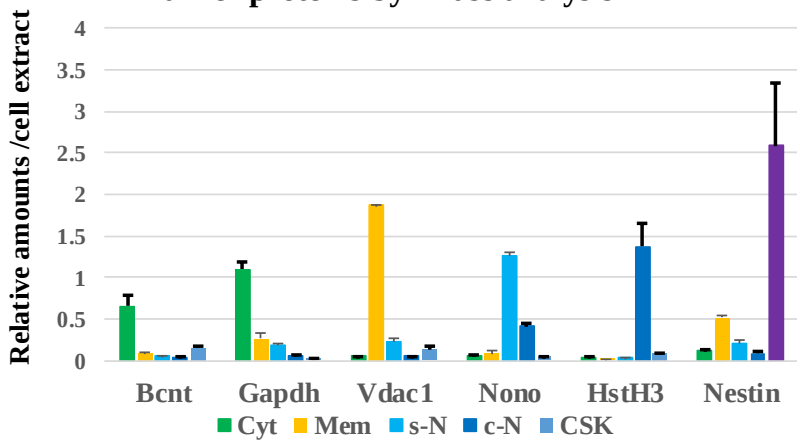

C

Paraspeckle components and Hnrnps

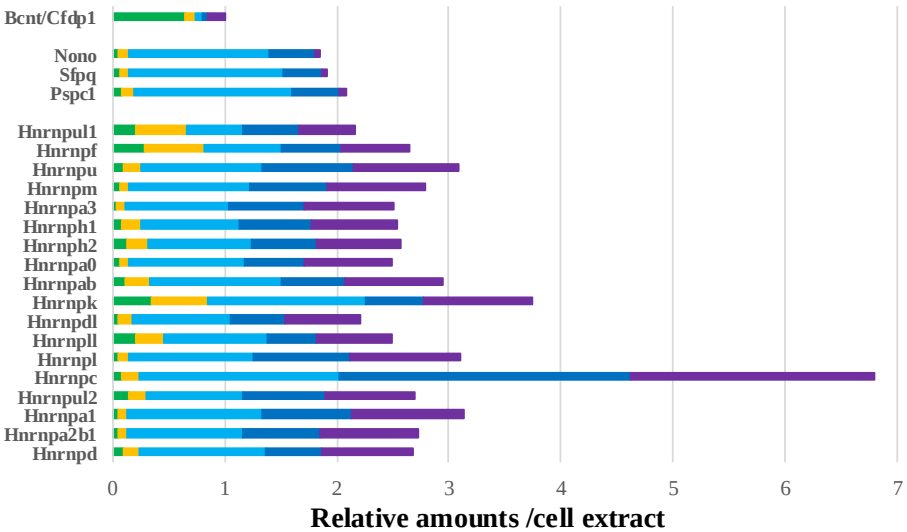

D

Six "nuclear proteins" detected in the cytoplasmic fraction

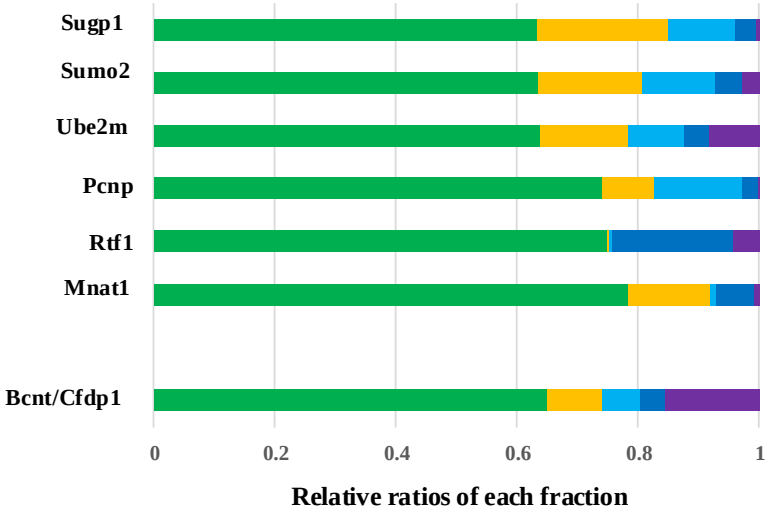

Figure 5

Release of Bcnt/Cfdp1 by digitonin treatment in an isotonic solution

A

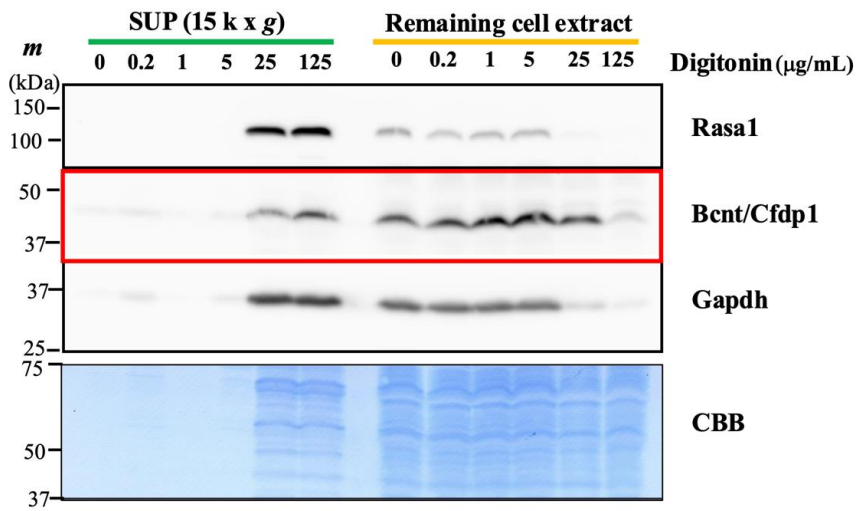

B

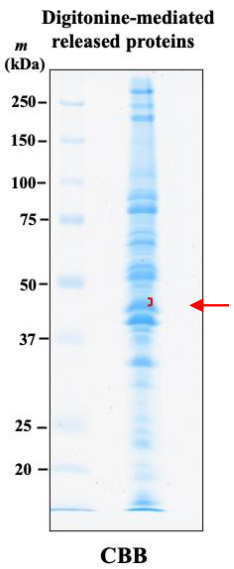

C

Gene Symbol	Bcnt/Cfdp1
Sum PEP Score	81.555
Coverage [%]	41
# Peptides	11
# PSMs	17
# Unique Peptides	11
Score Mascot: Mascot	531

D

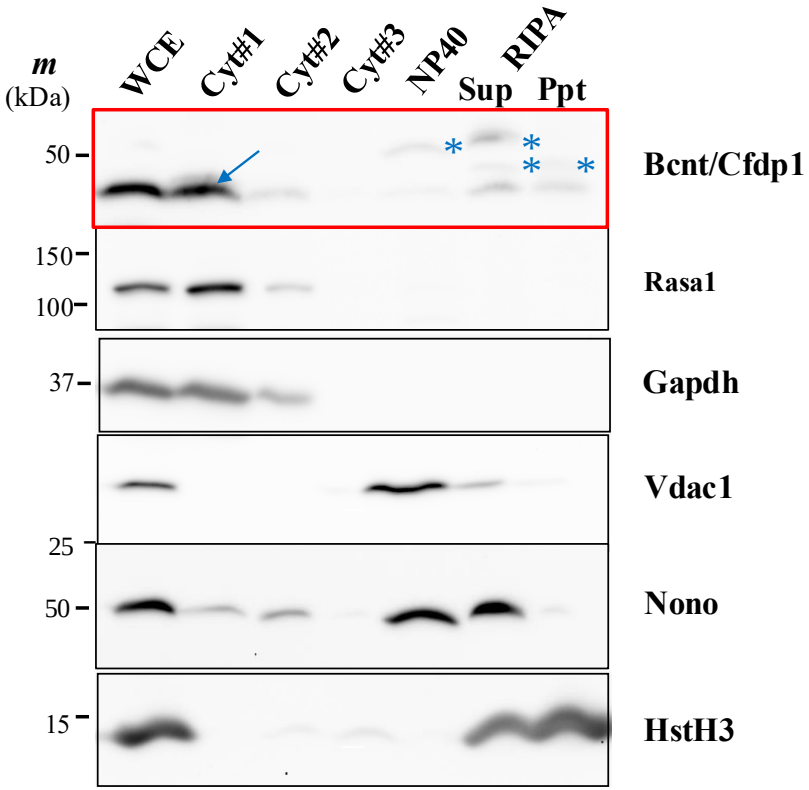

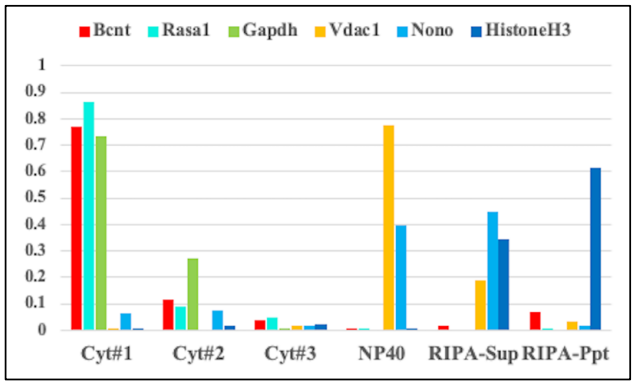

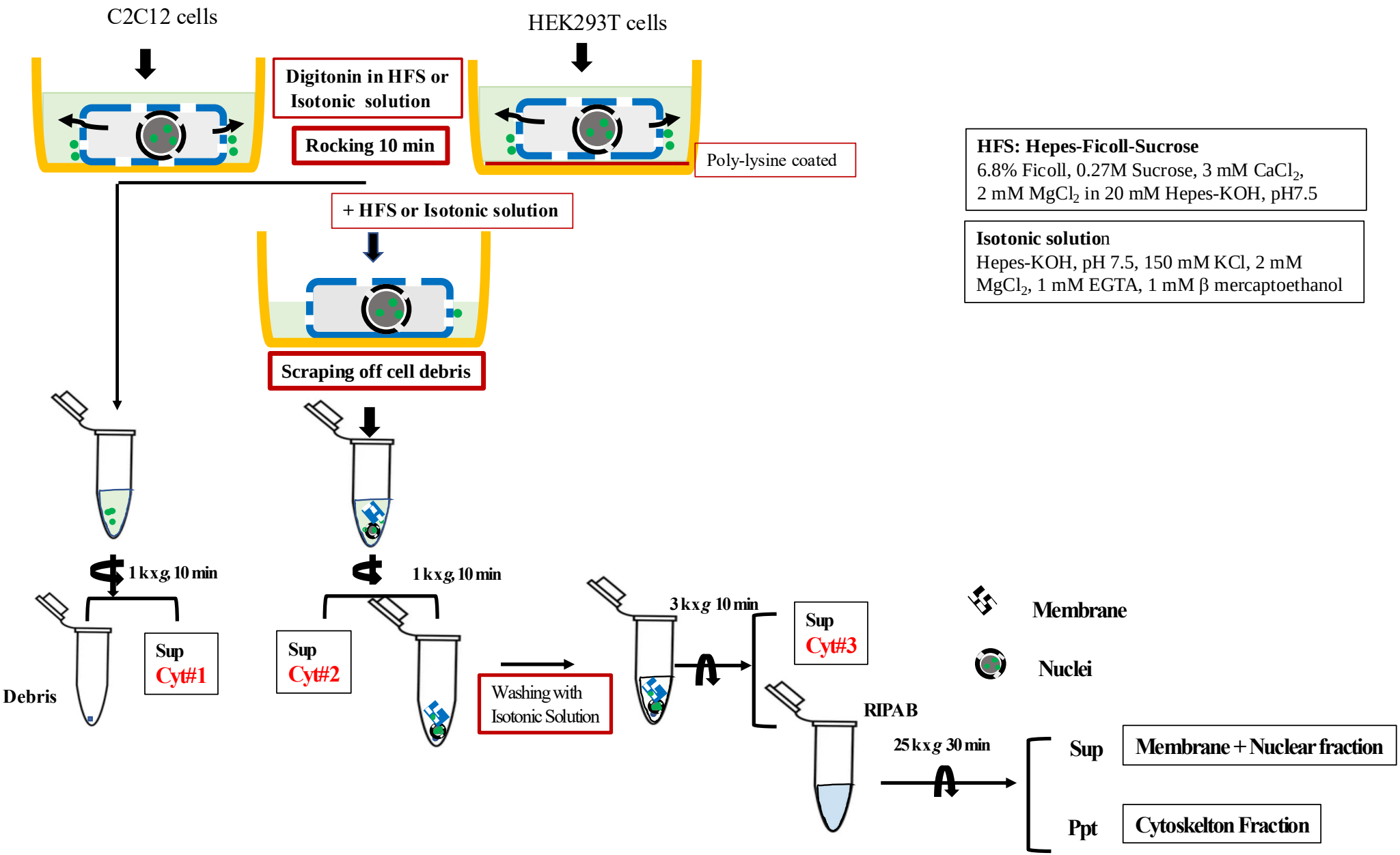

HFS: Hepes-Ficoll-Sucrose
6.8% Ficoll, 0.27M Sucrose, 3 mM $CaCl_2$,
2 mM $MgCl_2$ in 20 mM Hepes-KOH, pH7.5

Isotonic solution
Hepes-KOH, pH 7.5, 150 mM KCl, 2 mM $MgCl_2$, 1 mM EGTA, 1 mM β mercaptoethanol

Figure 7

Differential release of Bcnt/Cfdp1 from cytosolic proteins by digitonin treatment in HFS

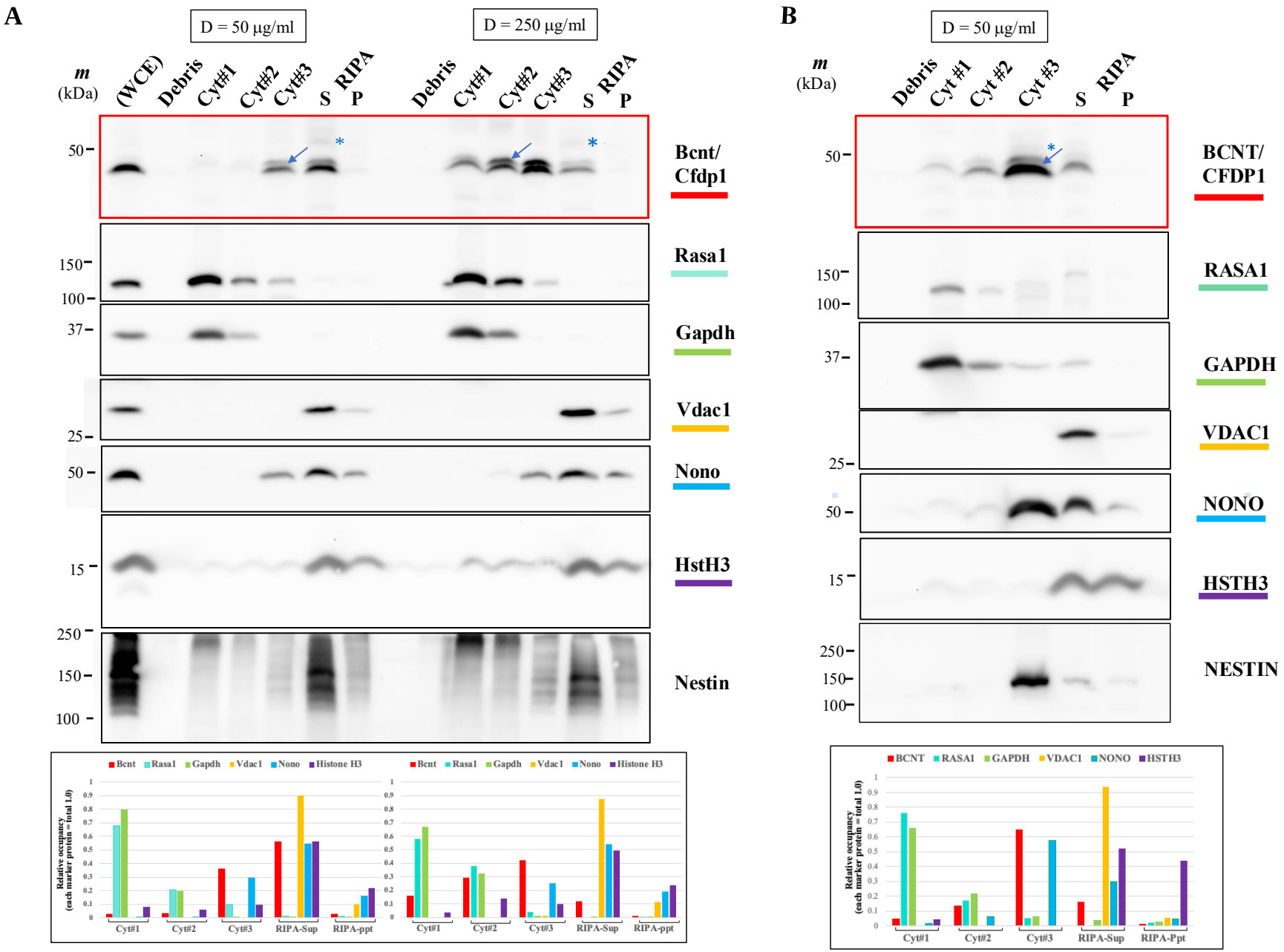

Figure 8
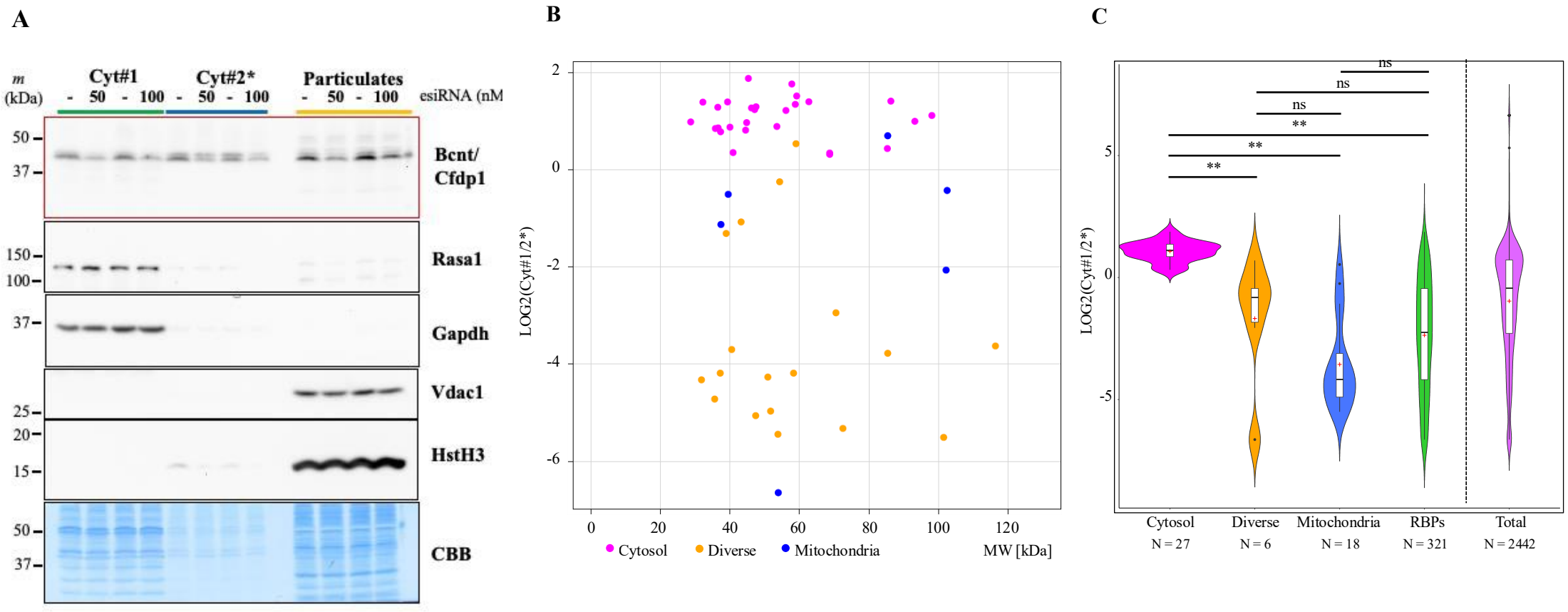
Mobility or integrity of digitonin-mediated released proteins in the Cytoplasm
-Evaluation from the ratios of two fractions-